Cell Reports

Article

Asymmetrical nucleosomal DNA signatures regulate transcriptional directionality

Graphical abstract

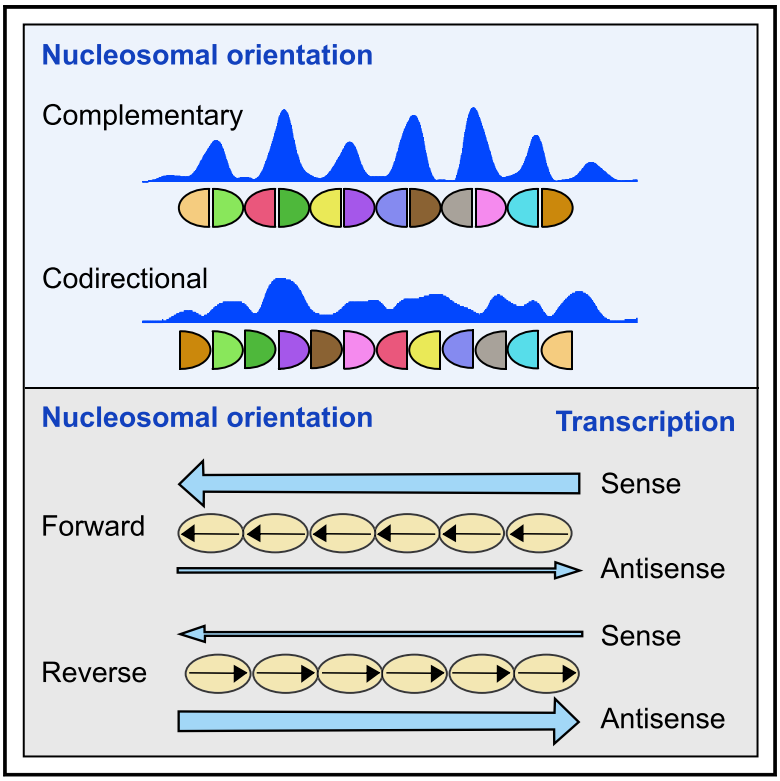

Authors

Alicia García, Laura Durán, Mar Sánchez, Sara González, Rodrigo Santamaría, Francisco Antequera

Correspondence

cpg@usal.es

In brief

García et al. show that nucleosomal signatures along genes are asymmetrical and that the proximal and distal halves of nucleosomal DNA contribute differentially to nucleosome stability *in vivo*. In the case of +1 nucleosomes, this asymmetry facilitates or hinders transcription depending on the orientation of its underlying DNA.

Highlights

- Nucleosomal signatures along transcription units are asymmetrical
- Proximal and distal nucleosomal DNA halves contribute differentially to nucleosome stability
- The forward or reverse orientation of +1 nucleosomal DNA facilitates or hinders transcription
- +1N signature confers asymmetrical accessibility of micrococcal nuclease to nucleosomes

García et al., 2024, Cell Reports *43*, 113605
January 23, 2024
https://doi.org/10.1016/j.celrep.2023.113605

CellPress

Cell Reports

CellPress
OPEN ACCESS

Article

Asymmetrical nucleosomal DNA signatures regulate transcriptional directionality

Alicia García,[1] Laura Durán,[1] Mar Sánchez,[1] Sara González,[1] Rodrigo Santamaría,[2] and Francisco Antequera[1,3,*]
[1]Instituto de Biología Funcional y Genómica (IBFG), CSIC–Universidad de Salamanca, Campus Miguel de Unamuno, 37007 Salamanca, Spain
[2]Departamento de Informática y Automática, Universidad de Salamanca/Facultad de Ciencias, Plaza de los Caídos s/n, 37007 Salamanca, Spain
[3]Lead contact
*Correspondence: cpg@usal.es
https://doi.org/10.1016/j.celrep.2023.113605

SUMMARY

Despite the symmetrical structure of nucleosomes, *in vitro* studies have shown that transcription proceeds with different efficiency depending on the orientation of the DNA sequence around them. However, it is unclear whether this functional asymmetry is present *in vivo* and whether it could regulate transcriptional directionality. Here, we report that the proximal and distal halves of nucleosomal DNA contribute differentially to nucleosome stability in the genome. In +1 nucleosomes, this asymmetry facilitates or hinders transcription depending on the orientation of its underlying DNA, and this difference is associated with an asymmetrical interaction between DNA and histones. These properties are encoded in the DNA signature of +1 nucleosomes, since its incorporation in the two orientations into downstream nucleosomes renders them asymmetrically accessible to MNase and inverts the balance between sense and antisense transcription. Altogether, our results show that nucleosomal DNA endows nucleosomes with asymmetrical properties that modulate the directionality of transcription.

INTRODUCTION

Nucleosomes are the basic structural units of chromatin upon which the three-dimensional organization of the genome is built. Comparative analyses among species have revealed that nucleosomes occupy specific positions relative to the DNA sequence that have been maintained across evolutionary timescales.[1] That stable association has left its imprint in the distribution of polymorphisms in phase with the nucleosomal profile in yeast and *Drosophila*[2,3] and has contributed to the emergence of new exons in the human genome.[4]

Nucleosomal organization relies on ATP-dependent remodeler complexes that facilitate the displacement, eviction, or replacement of histones in nucleosomes.[5,6] Removal of specific remodelers disarranges the nucleosomal order, deregulates transcription, and causes unscheduled antisense expression.[7–13] Histone chaperones and histone-modifying enzymes also contribute to maintaining nucleosomal order and regulate transcription in the chromatin context.[14–17] An additional determinant of nucleosome positioning is the DNA sequence. The tight wrapping of 147 bp of double-stranded DNA around the histone core imposes a strong bending along the axis of the molecule and distorts the spacing and twist between adjacent nucleotides, especially in sites where the minor groove contacts the octamer surface.[18,19] This implies that different DNA sequences have different energetic requirements to maintain a stable DNA-histone interaction,[19–21] and several studies have revealed that, despite the symmetrical structure of the histone octamer, sequence differences between the two halves of nucleosomal DNA endow nucleosomes with asymmetrical properties.[22–27] For example, single-molecule analyses using optical tweezers have shown that the force required to unwind the two DNA strands differs between the two ends of nucleosomal DNA. These properties depend on sequence elements asymmetrically located in the two halves of nucleosomal DNA, since their swapping inverts the resistance to unwinding.[22] These observations parallel previous results that mononucleosomes offer different resistance to the passage of RNA polymerase II (RNA Pol II) depending on the polarity of transcription.[28] As in the case of unwinding, detailed dissection of the nucleosomal barrier showed that RNA Pol II pausing depends on sequences asymmetrically located relative to the nucleosomal dyad.[29–34] Altogether, this evidence supports that, despite the symmetrical structure of the histone octamer, specific sequence elements on the distal and proximal regions of mononucleosomal DNA can confer asymmetrical properties to nucleosomes. Most of those studies, however, were done *in vitro* and, for technical reasons, focused on a small number of nucleosomes. Therefore, it is unclear whether these sequence-dependent polarized properties of nucleosomes are present in the genomic context and whether they could contribute to the regulation of transcription directionality. We have shown that nucleosomal signatures contain information to target nucleosomes to specific positions on natural and

artificial DNA molecules *in vivo*.[35,36] Here, we report that nucleosomal signatures along genes in the fission yeast *Schizosaccharomyces pombe* are asymmetrical and uncover an unsuspected layer of information of nucleosomal DNA that facilitates or hinders the passage of RNA polymerase to regulate the polarity of transcription.

RESULTS

Asymmetrical nucleosome signatures and RNA polymerase pausing along transcription units

Nucleosome signatures were initially described as symmetrical, because they were derived from nucleosomes along coding and non-coding genomic regions without taking into account the directionality of transcription (Figure 1A, genome average charts).[35] In this case, the distribution of the A and C nucleotides is mirrored by the distribution of T and G, respectively, along the same strand of DNA relative to the dyad. This implies that the two strands of nucleosomal DNA are palindromic in terms of base composition and that the amount of A and C is higher than T and G in the 5′ compared with the 3′ region of each strand. However, in view of the mounting evidence of nucleosomal DNA asymmetry commented on in the introduction, we wondered whether the A and C signatures would remain symmetrical to T and G when taking into account the polarity of transcription.

To test this possibility, we selected seven non-overlapping groups of nucleosomes along genes in *S. pombe* and represented their signatures relative to the direction of transcription. Figure 1A (top row) shows that the distribution of the four nucleotides in the seven groups was asymmetrical relative to the dyad position. Asymmetrical signatures are also detectable in the phylogenetically distant yeast *S. cerevisiae* (Figure 1A, bottom row) and in *Candida albicans* and two other species of *Schizosaccharomyces* (Figure S1A), although their profiles are different from those in *S. pombe*, as expected from the species specificity of nucleosomal signatures.[35] Asymmetry was more pronounced in the first nucleosome (+1N) than in downstream nucleosomes in all the species tested, especially in its promoter-proximal half. Since −1 nucleosomes (−1N) also flank promoters, we have examined their signature in *S. pombe*. Figure S1B shows that the distribution of the four nucleotides is also asymmetrical but different from that of +1N, suggesting that they could confer distinctive properties to +1N to facilitate transcription from unidirectional promoters.

Experiments on single nucleosomes *in vitro* have shown that RNA Pol II pauses at specific positions along nucleosomes.[28,31,34,38,39] To test whether pausing also occurs in *S. pombe in vivo*, we mapped the position of active RNA Pol II sites reported by Booth et al.[37] onto the seven groups of nucleosomes. Figure 1B shows a prominent peak of RNA Pol II upstream of the dyad of +1N, as previously reported,[37] but we also found higher polymerase occupancy in the proximal half of each group of downstream nucleosomes relative to the transcription start site (TSS), indicating that RNA Pol II pauses *in vivo* before reaching the nucleosomal dyad in *S. pombe* as has been reported in *S. cerevisiae*.[40]

The two halves of mononucleosomal DNA contribute differentially to nucleosome positioning

In vitro experiments have shown that RNA Pol II pausing is important to generate an intranucleosomal DNA loop during transcription to maintain the position of nucleosomes relative to the DNA sequence.[29,31,33,34,41] The formation of this loop depends on DNA sequences in the distal half of nucleosomal DNA relative to the TSS, making it possible that the two halves might contribute differentially to the stability of nucleosomes.[30] To test this, we modified the proximal and distal halves of nucleosomal DNA along the *S. pombe ura4* and *his7* genes to evaluate the consequences on the stability of their nucleosomal pattern and transcription *in vivo*. We selected these two genes as models because they are non-essential in *S. pombe* and they are organized in arrays of well-positioned nucleosomes in wild-type cells (Figure 2A, WT). We have reported that replacing codons with synonymous codons in nucleosomal DNA alters the nucleosomal positioning profile along genes.[36] To test the individual contributions of the proximal and distal halves to positioning, we constructed four *S. pombe* strains in which we replaced 17 codons with synonymous codons between positions −10/−61 (distal) and +10/+61 (proximal) relative to the dyad and to the TSS of each nucleosome along the open reading frames (ORFs) of the *ura4* and *his7* genes. Micrococcal nuclease sequencing (MNase-seq) occupancy maps showed that changes in the proximal half of nucleosomal DNA generated a nucleosomal profile and a distribution of MNase cuts comparable to that of the wild type (Figures 2A and S2). Quantitative analysis of positioning using DANPOS[42] showed that the fuzziness of only one nucleosome in each gene was higher than in the wild-type pattern. In contrast, modification of the distal half altered the position of five nucleosomes in each of the *ura4* and *his7* genes relative to the wild type and reduced their occupancy, mostly in *ura4*, where the alteration in nucleosome positioning was more severe (Figures 2A and S2). We have made biological duplicates of the occupancy maps of all the strains in this work, and we have compared them by the size distribution of MNase fragments and the concordance of nucleosome fuzziness and by direct comparison of several specific genomic regions. Results in Figures S3 and S4 show that differences between replicates fall within the range of experimental variation.

Expression analysis of the two *ura4* and *his7*-modified strains showed that disruption of the nucleosomal pattern in the distal strain correlated with a strong downregulation of their expression, indicating that the loss of positioning was not caused by overexpression, as happens in highly transcribed genes in *S. pombe*.[43] By contrast, expression in the *ura4* and *his7* proximal strains was similar to that of wild type, consistent with their less-altered nucleosomal profiles (Figure S5A). Analysis of mRNA stability by thiolutin showed that differences in expression between the proximal and the distal strains are not due to a lower RNA stability of the distal RNAs[44] (Figure S5B).

Given that the ORF of *ura4* starts approximately in the center of the +1N nucleosome, it was not possible to modify the proximal half of its DNA by codon substitution. This implied that the sequence underlying +1N remained unmodified in the proximal strain (Figure 2A, *ura4* proximal), while its distal half was modified in the distal strain (Figure 2A, *ura4* distal). This left open the

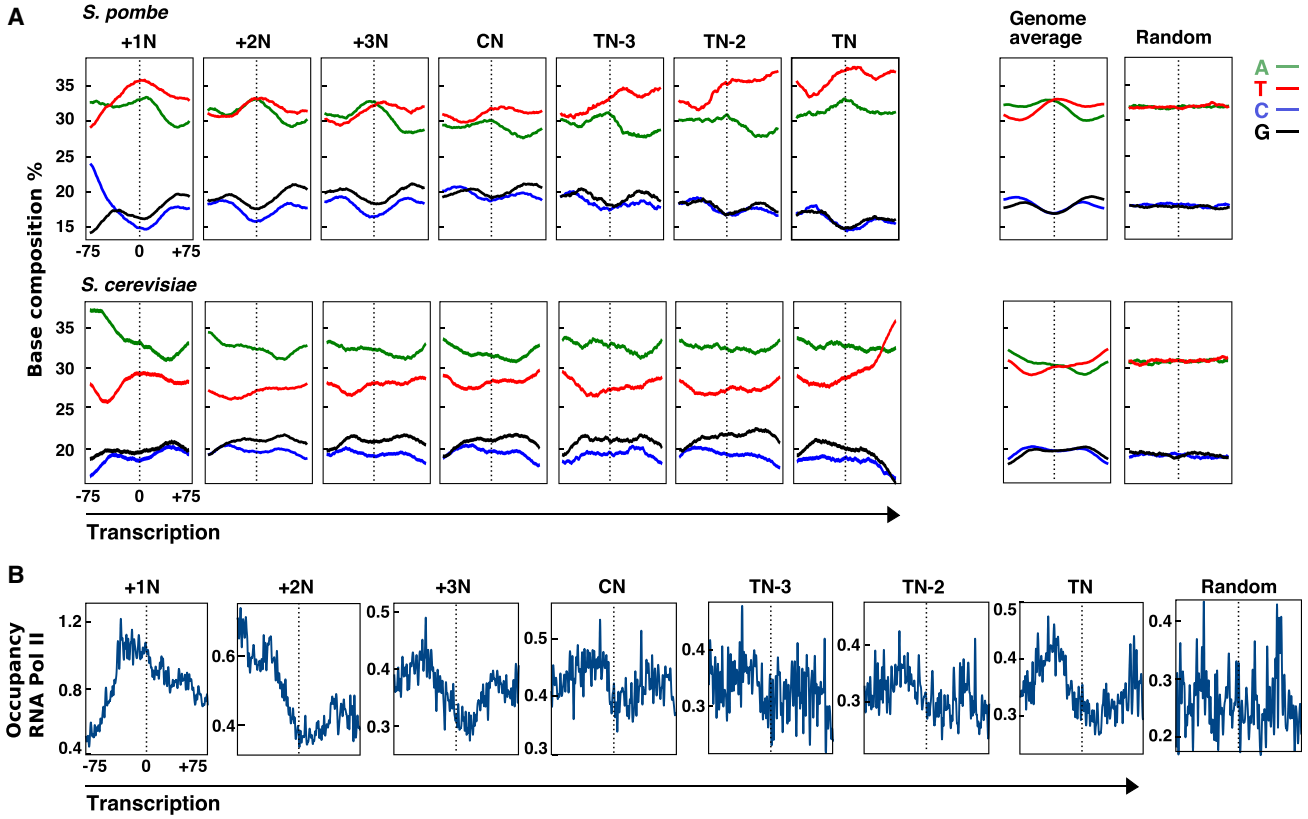

Figure 1. Asymmetrical nucleosomal signatures and RNA polymerase pausing along transcription units

(A) Base composition along DNA of *S. pombe* and *S. cerevisiae* nucleosomes overlapping the transcription initiation (+1N) and termination (TN) sites. +2N and +3N represent the two nucleosomes immediately downstream of +1N, and TN−2 and TN−3 the two nucleosomes immediately upstream of TN. CN indicates nucleosomes in the central position of transcription units. The average number of nucleosomes analyzed in each group was 2,600 and 2,700 in *S. pombe* and *S. cerevisiae*, respectively. The arrow indicates the direction of transcription. The genome average charts show the aggregated signatures of nucleosomes in genes and intergenic regions genome-wide without considering transcription directionality. The random charts indicate the nucleotide distribution along 2,700 DNA regions of 147 bp selected at random along each genome. Vertical dotted lines indicate the dyad position in each group of nucleosomes. The x axis spans ±75 bp from the dyad in each chart.

(B) Pausing sites of RNA Pol II accumulate in the proximal half of nucleosomes relative to the transcription initiation site in the seven groups shown in (A). The relative occupancy of RNA Pol II scale is different in +1N and downstream nucleosomes and was normalized relative to the spike-in average genome as described by Booth et al.[37] The random chart represents the distribution of pausing sites in 660 sequences of 150 bp selected at random in the genome. The dyad position and the direction of transcription are indicated as in (A).

possibility that the disorganized nucleosome pattern in the distal strain could be a consequence of the loss of positioning of +1N. To test this, we constructed another strain in which we modified the distal half of +1N in the proximal strain. The MNase-seq map showed that occupancy of +1N was drastically reduced in this strain, while the positioning of downstream nucleosomes 2–6 was similar to that of the proximal and wild-type cells (Figure 2A, proximal (+1N) and Figure S2). RNA expression in this case was intermediate between the level of the proximal and the distal strains (Figure S5A). Altogether, these results indicated that the two halves of nucleosomal DNA along genes contribute differentially to nucleosome positioning and transcription and that positioning of downstream nucleosomes does not depend on the correct positioning of +1N.

These results raised the questions of whether the differential contribution of the two halves of nucleosomal DNA was a general property of nucleosomes and whether each half encoded different and complementary positioning information. To test these questions, we replaced the DNA region encompassing the six nucleosomes along the *ura4* gene (bracket in Figure 2A) by six fragments of 150 bp, each generated by combining the proximal and distal halves of unrelated nucleosomes from different genes selected at random in the genome (Figure 2B, complementary). Occupancy maps showed that these chimeric nucleosomal DNA fragments specified a regular positioning pattern virtually identical to that of the endogenous *ura4* nucleosomes that they replaced. By contrast, this pattern was completely lost if the same sequences of the six proximal and distal halves were arranged in the same orientation (Figure 2B, codirectional, and Figure S6). These results indicate that the two halves of nucleosomal DNA contribute differentially and complementarily to nucleosome positioning and that this is a general property of nucleosomes along transcription units. The sequence of each half of the nucleosomal DNA and their

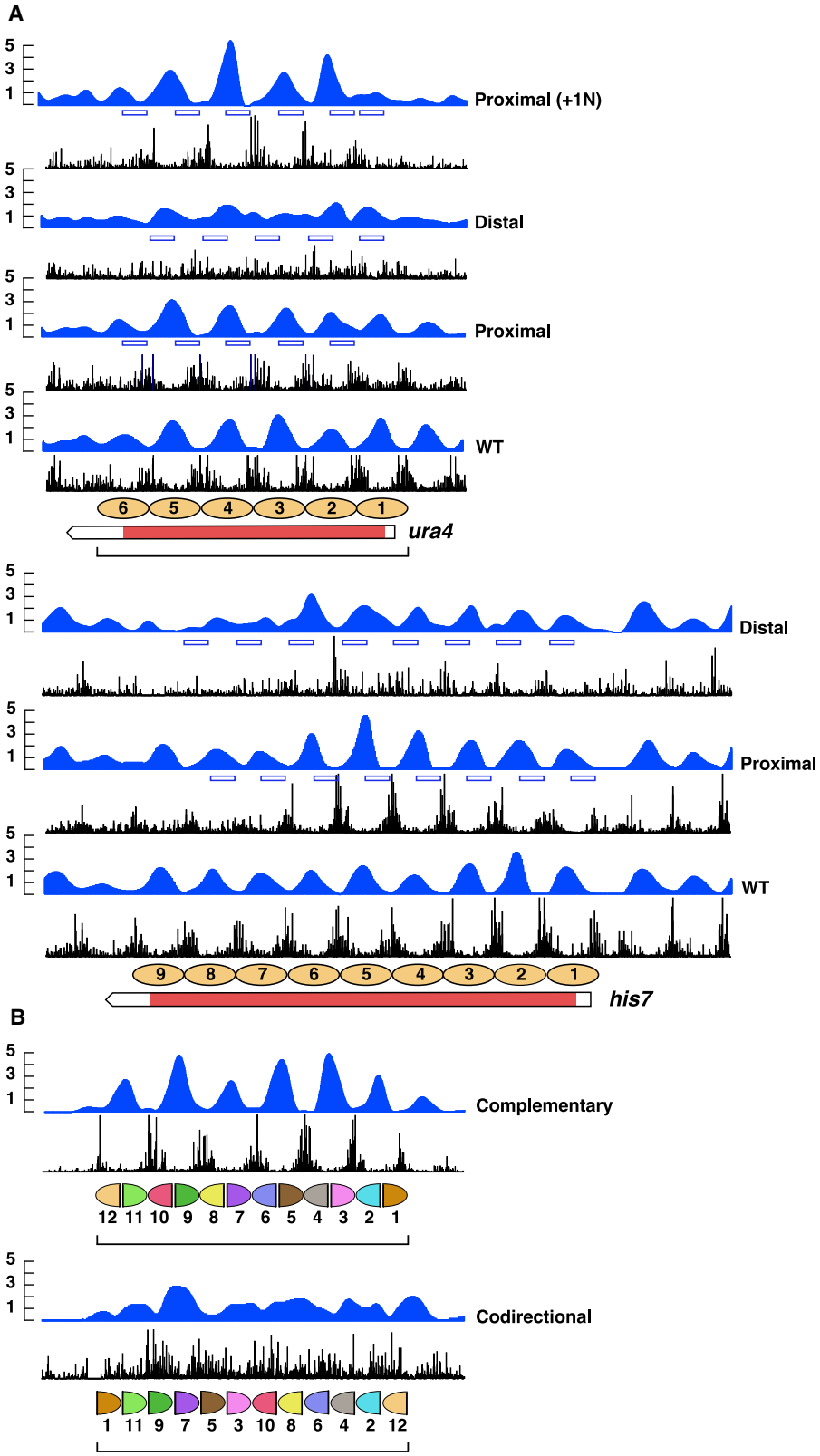

(legend on next page)

endogenous positions in the genome are indicated in Table S1. Biological replicates of all the maps in Figure 2 are shown in Figure S7.

The orientation of nucleosomal DNA regulates transcription directionality

Given the asymmetrical contribution of mononucleosomal DNA to nucleosomal positioning (Figure 2) and the accumulation of RNA Pol II in the proximal half of +1N and downstream nucleosomes (Figure 1B), we asked whether the orientation of nucleosomal DNA relative to the directionality of transcription would be functionally relevant. To address this question, we synthesized two chimeric constructs (+1N-A and +1N-B), each made up of eight +1 nucleosomal DNA fragments derived from 16 *S. pombe* genes selected at random, maintaining the same orientation relative to transcription as in their endogenous loci. We also synthesized another two fragments of the same size (CN-A and CN-B) from nucleosomes in the central position of another 16 genes, also maintaining the same orientation (Figure 3A; Table S1). We used these four constructs to replace a genomic region of the same size encompassing eight well-positioned nucleosomes along the *S. pombe SPAC11D3.16c* non-essential gene. Each construct was inserted in the two orientations to generate eight strains that maintained the endogenous nucleosome-depleted promoter region of *SPAC11D3.16c* (Figure 3A). Since the chimeras were created by assembling unrelated genomic DNA fragments, none of them included any ORF spanning its entire length.

We measured transcription of the eight constructs on total RNA using primers at their 3′ end to synthesize the cDNAs prior to qPCR (arrowhead in Figure 3A). Results in Figure 3B (3′ bar charts) show that the level of transcripts of the reverse +1N-A and +1N-B constructs was strongly reduced relative to the forward versions. We also detected that transcription of +1N-B was about 10-fold lower than that of +1N-A, although both were expressed from the same promoter. To explore the causes of this difference, we repeated the analysis using cDNA primers approximately 200 bp downstream of the transcription initiation site (arrowhead in Figure 3A). In this case, the level of transcription was similar in the forward and reverse +1N-A and +1N-B (Figure 3B, 5′ bar charts), indicating that RNA Pol II reaches the 3′ end of +1N-B less efficiently than that of +1N-A. This is likely due to differences in the sequence of the constructs, since the stabilities of the corresponding RNAs were comparable (Figure S8A). This difference in transcription at the 3′ end of +1N-B correlates with a lower value of the ratio of Ser2/total RNA Pol II in +1N-B relative to +1N-A (Figure 3D). Figure 3D also shows that the ratio Ser2-P/total RNA Pol II declines from 5′ to 3′ in the reverse +1N-A and +1N-B, in line with the downregulation of transcription in the same constructs. A possible explanation for the similar levels of transcription at the 5′ end in the forward and reverse +1N-A and +1N-B is that the two specific +1 nucleosomes of the two constructs, which we selected from two genes chosen at random in the genome (Table S1), do not affect transcription significantly in the reverse orientation. It is likely that individual +1 nucleosomes will vary in their potential to allow or disfavor transcription because the mechanical properties of bending will depend on their DNA sequence. It is possible that the strong transcription downregulation at the 3′ end of the reverse +1N-A and +1N-B is due to the cumulative effect of the eight nucleosomes that make up each construct. A second and non-exclusive possibility is that the +1 nucleosome in the reverse orientation might allow the RNA polymerase to escape the promoter before complete maturation of the preinitiation complex, whose effect could be undetectable on the +1 nucleosome but would result in defective elongation or premature termination along the reverse constructs.

By contrast, in the case of central nucleosomes, only CN-A showed a small decrease in transcription in the reverse relative to the forward construct in total RNA that was not detected in nascent RNA (see below) (Figures 3B and 3C), consistent with a similar ratio of Ser2-P/total RNA Pol II in the 5′ and 3′ regions of CN-A and CN-B (Figure 3D). The individual distributions of total and Ser2-P RNA Pol II are shown in Figure S9.

To confirm the differences in transcription between the forward and the reverse constructs, we isolated nascent RNA after a 6 min pulse with 4-thiouracil using a fixed amount of labeled *S. cerevisiae* nascent RNA as spike-in for normalization.[45] Results in Figure 3C show a reduction in transcription in the reverse +1N-A and +1N-B relative to their forward versions, similar to that found on total RNA. This approach also detected the reduced level of transcription at the 3′ end of +1N-B relative to +1N-A. We found no differences between CN-A and CN-B forward and reverse nascent transcripts (Figure 3C), also consistent with the results on total RNA. We have not detected any antisense transcription in any of the eight chimeric constructs nor in the *SPAC11D3.16c* wild-type gene, in agreement with published datasets of transcription in *S. pombe*[46] (www.pombase.org).

To assess whether the resulting chimeras adopted the nucleosome profile predicted by their constituent units, we generated duplicate maps of nucleosomal occupancy of the eight strains. In all cases, the eight nucleosomes in their ectopic localization displayed a well-positioned profile along the forward and reverse constructs (Figure S8C). Altogether, these results imply that

Figure 2. The two halves of mononucleosomal DNA contribute differentially to nucleosome positioning

(A) Nucleosome occupancy map (blue) and distribution of MNase cutting sites (black vertical lines) along the *S. pombe ura4* and *his7* genes normalized to the genome average. Blue rectangles indicate the modified proximal or distal halves relative to the TSS in the proximal and distal strains, respectively, and numbered orange ovals represent nucleosomes along the wild-type *ura4* and *his7* genes (WT). Pointed rectangles and red bar spans represent the *ura4* and *his7* transcripts and ORFs. In the proximal (+1N) strain (top diagram), the distal half of +1N and the proximal half of downstream nucleosomes were modified. All maps are shown at the same scale of nucleosomal occupancy shown on the left.

(B) The DNA region encompassing six nucleosomes along the *ura4* gene (bracket in A) was replaced by a DNA fragment of the same size made up of six complementary halves from 12 nucleosomes selected at random in the genome (brackets). In the complementary strain, halves maintain the same orientation as in their endogenous *loci*, and in the codirectional strain, halves are arranged codirectionally as indicated by their color and number. The genomic origin of each fragment is indicated in Table S1.

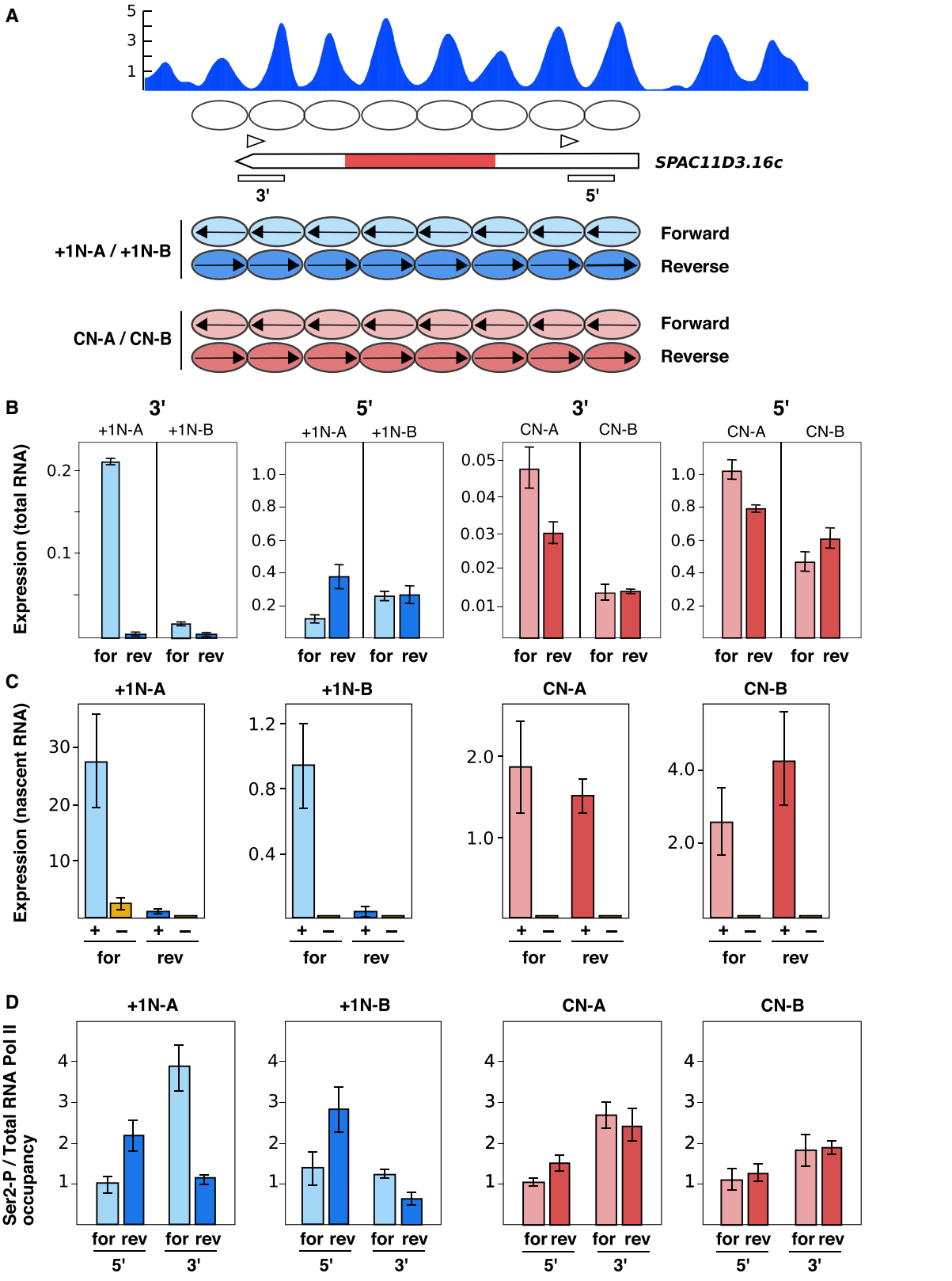

(legend on next page)

the wild-type (forward) orientation of +1 nucleosomal DNA is permissive for transcription, while its reverse orientation restrains it. This effect seems to be specific for +1 nucleosomes, since parallel analyses did not detect significant differences in downstream nucleosomes regardless of their orientation.

The polarity of DNA-encoded nucleosomal signatures modulates the balance between sense and antisense transcription

The different impacts of the orientation of +1N nucleosomal DNA on transcription raised the question of whether the +1N signature could confer the properties of +1 nucleosomes to other nucleosomes. To test it, we incorporated the +1N signature in the two orientations in the nucleosomes along the *ura4* and *his7* genes (Figure 4A) and measured transcription in the four modified strains. Signatures can be incorporated into nucleosomal DNA along ORFs by replacing each codon in the sequence to be modified by the synonymous codon with the highest score in the corresponding position in the matrix that defines the signature to be incorporated. This matrix contains the frequency of each dinucleotide along the 147 bp of +1N nucleosomal DNA derived from thousands of +1 nucleosomes (see Quintales et al.[35] and González et al.[36] and STAR Methods for details). The resulting modified nucleosomal sequence mimics the +1N signature as closely as allowed by the degeneracy of the genetic code and continues to encode the wild-type protein.

Measurement of the level of sense RNA of the *ura4* and *his7* genes harboring the reverse +1N signature revealed a 4- and 3-fold decrease, respectively, relative to the +1N forward versions (Figure 4B, *ura4* (S) and *his7* (S)), suggesting that the asymmetrical signature of +1N contains directional information that favors transcription in the wild-type (forward) orientation and downregulates it in the reverse. Analysis of RNA stability by thiolutin showed slightly higher values for the forward version of the *his7* mRNA (Figure S8B) that could partially contribute to the differences in the level of sense RNA. Since the *ura4* gene, along with many other genes, is induced in the presence of thiolutin,[47] we took advantage of the fact that this gene is rapidly repressed upon removal of glucose from the medium[48] to measure the decline of its mRNA under these conditions. Results in Figure S8B show that the stability of the reverse-construct RNA was slightly higher than that of the forward construct.

The wild-type *ura4* and *his7* genes are adjacent to two convergent genes, *tam14* and *ccc2*, respectively, whose transcripts overlap with the sense transcripts of the two genes.[46] We took advantage of this fact to test whether the reverse remastered strains would be more permissive than the forward to antisense transcription. Figure 4B (*ura4* (AS)) shows that antisense *ura4* increased dramatically in the reverse construct relative to the forward and also in the *his7* gene, although in a lower proportion (*his7* (AS)).

To confirm these differences in expression between the forward and the reverse constructs of *ura4* and *his7*, we measured transcription on nascent RNA in the four strains by 4-thiouracil labeling as in Figure 3C. Results in Figure 4C (*ura4* (S)) show that sense transcription in the forward and reverse *ura4* strains was not significantly higher than in the non-labeled control, probably due to a low rate of RNA synthesis during the short 6 min pulse of 4-thiouracil, in agreement with the very low level of transcripts detected in the two strains in total RNA (Figure 4B, *ura4* (S)). Antisense transcription, however, was clearly higher in the reverse than in the forward construct (Figure 4C, *ura4* (AS)), also in agreement with the differences found on total RNA (Figure 4B, *ura4* (AS)). In the case of *his7*, sense transcription was higher in the forward than in the reverse construct (Figure 4C, *his7* (S)), while the opposite was found for antisense transcription (Figure 4C, *his7* (AS)), also consistent with the results on total RNA (Figure 4B, *his7* (S) and (AS)). Antisense transcription is also detectable in the *ura4* and *his7* genes in wild-type cells, but their level is approximately 30- and 300-fold lower than the sense, respectively (Figure S5C).

The mirror image distribution of total and active Ser2 RNA Pol II along the forward and reverse *ura4* genes (Figure 4D, *ura4*) is probably due to the low level of sense transcription described above (Figure 4C). In *his7*, sense transcription was higher than in *ura4*, and the levels of total and Ser2 RNA Pol II increased from 5′ to 3′, although the increase was lower in the reverse than in the forward construct (Figure 4D, *his7*). Altogether, these results show that the +1N signature contains information such that it is more permissive to sense transcription when is incorporated into the forward than into the reverse orientation along the *S. pombe ura4* and *his7* genes, while incorporation in the reverse orientation favors antisense transcription.

Since we modified the nucleosomal DNA sequences of all the nucleosomes along the entire *ura4* and *his7* ORFs, we wondered

Figure 3. The orientation of nucleosomal DNA regulates transcription directionality

(A) Nucleosome occupancy map of the *SPAC11D3.16C* gene of *S. pombe* (blue). Scale on the left indicates occupancy relative to the genome average. White ovals represent nucleosomes, the pointed rectangle indicates the transcript, and the red bar indicates the ORF. White bars below the genes represent the 3′ and 5′ amplicons analyzed by ChIP in (D). Arrowheads indicate the positions of the 3′ and 5′ cDNA primers. Blue ovals represent the two constructs (+1N-A and +1N-B) made up of 16 fragments of nucleosomal DNA derived from +1N nucleosomes in the forward (light blue) and reverse (dark blue) orientation relative to transcription in their endogenous loci. The same applies to the light and dark red ovals but using nucleosomal DNA from the central nucleosomes of 16 genes selected at random (CN-A and CN-B).

(B) Expression of each construct in the forward and reverse orientation using the 3′ and 5′ primers indicated in (A) to synthesize the cDNAs from total RNA. Expression was normalized to the *S. pombe* actin *act1* gene. Histograms represent the average of two or three biological replicates per sample.

(C) Expression of the same constructs using the same 3′ primers as in (B) but using nascent RNA as a template (+ histograms). Values were normalized to the *ACT1* gene of *S. cerevisiae* as a spike-in control of nascent RNA. The − histograms indicate transcription on RNA isolated without 4-thiouracil labeling. Values represent the average of two biological replicates.

(D) Ratio of active (Ser2-P) versus total RNA Pol II occupancy measured by ChIP normalized to input chromatin and to a non-transcribed region of the *S. pombe* mating locus. 5′ and 3′ in the x axis refer to the 5′ and 3′ amplicons of the eight strains shown in (A). Histograms in (B) and (D) represent averages of three or four biological replicates per sample. Error bars indicate standard deviation. Student's t test p values of all the comparisons are shown in Table S2.

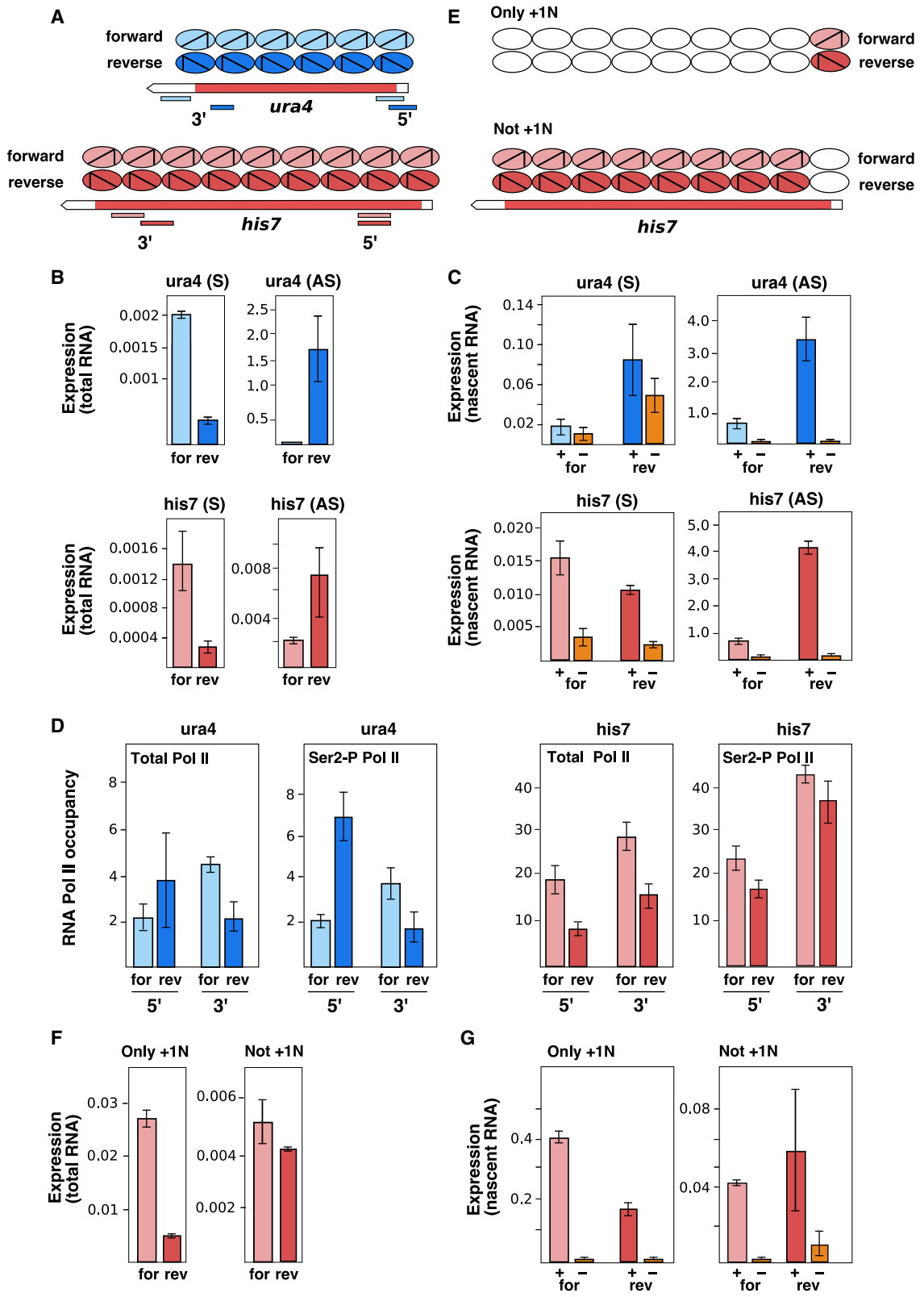

(legend on next page)

whether the reverse orientation of the +1N by itself would downregulate transcription or whether downstream nucleosomes would also contribute to it. To test the independent contribution of the two groups of nucleosomes, we generated two strains in which we incorporated the +1N signature in the two orientations into the first nucleosome of *his7* while maintaining the wild-type sequence in the remaining eight nucleosomes downstream (Figure 4E, only +1N). For comparison, we generated two additional strains in which we maintained the wild-type version of the first nucleosome but introduced the +1N signature in the two orientations into the downstream nucleosomes (Figure 4E, not +1N). Figure 4F shows that incorporation of the reverse +1N signature into the only +1N strain reduced transcription by 80% relative to the forward version, while in the not +1N strain, downregulation was non-significant. Analysis of nascent RNA labeled with 4-thiouracil showed similar differences in the only +1N strain but detected no significant differences in the not +1N strain (Figure 4G). These results indicate that the asymmetry of the signature encoded in the 147 bp sequence of +1 nucleosomal DNA favors or restrains transcription depending on its orientation, even when incorporated only in the +1 nucleosome. However, the effect is undetectable under the same conditions when the reverse signature is incorporated only into downstream nucleosomes, highlighting the key role of the asymmetrical signature of +1N in transcriptional regulation.

Asymmetrical accessibility of +1 nucleosomes to MNase

The asymmetrical contribution of nucleosomal DNA to nucleosome stability (Figure 2) opened the possibility that the DNA-histone interaction could also be different in each half. To test this, we measured the accessibility to MNase along the 147 bp of nucleosomal DNA around the histone core in the seven groups of nucleosomes in Figure 1A. After chromatin digestion with MNase, we isolated DNA fragments without a size-selection step[49] and mapped the distribution of the end of subnucleosomal fragments included between positions −75 and +75 relative to the dyad. Histograms in Figure 5A show that the distributions of 5′ and 3′ ends in +1N was asymmetrical relative to the dyad position. This asymmetry, however, was not detectable in +2N and terminal (TN) nucleosomes (Figure 5A) or in any of the remaining groups of nucleosomes along the transcripts. Differences in the distribution of MNase ends are also evident in the +20/−20 region surrounding the dyad position of +1N (Figure 5B). To analyze the accessibility of each nucleosomal half independently, we selected subnucleosomal fragments exclusively derived from the proximal and distal halves (fragments not spanning the dyad position) of the seven groups of nucleosomes in Figure 1 and analyzed the distribution of 5′ and 3′ ends in each of them. Figure 5C shows that the asymmetrical distribution of MNase cuts of +1 nucleosomes is detectable only in their proximal half. Similar differences were detected using a 3.5-fold lower amount of MNase relative to the amount in Figure 5 (Figure S10A). Asymmetry in +1 nucleosomes was not due to a sequence bias of the MNase, since the distribution of cuts along the same sequences on naked DNA partially digested with MNase showed a symmetrical distribution of cuts along the corresponding mononucleosomal regions and in the proximal and distal halves (Figure S10B).

To test whether the asymmetric accessibility to MNase of +1N was influenced by its proximity to the nucleosome-depleted regions (NDRs) present in many *S. pombe* genes,[43,50] we ranked genes by the size of their 5′ NDR and analyzed the distribution of MNase cuts in the top 1,000 +1 nucleosomes associated with NDRs and in the bottom 1,000 that are not (Figure 5D). Figure 5E, NDR, shows that the pattern of MNase cuts in the proximal half was equally asymmetric in both groups, indicating that it was not favored by the proximity to an NDR.

In *S. cerevisiae*, asymmetric accessibility to MNase and to chemical cleavage in +1N has been correlated with the presence of the Remodeling the Structure of Chromatin (RSC) complex and of the H2A.Z histone.[51] To test whether this correlation was also detectable in *S. pombe*, we ranked +1 nucleosomes according to their enrichment in RSC or H2A.Z using the chromatin immunoprecipitation (ChIP) datasets of Lee et al.[52] and Clement-Ziza et al.,[53] respectively (Figure 5D). Figure 5E shows that, in both cases, the asymmetric accessibility to MNase of +1N was maintained in the 1,000 top and bottom groups of +1 nucleosomes, indicating that it was not caused by the presence of RSC or H2A.Z. To confirm these results, we generated libraries of subnucleosomal fragments in the *S. pombe rsc1*Δ mutant lacking the Rsc1 subunit of RSC and in the *pht1*Δ mutant

Figure 4. The polarity of DNA-encoded nucleosomal signatures modulates the balance between sense and antisense transcription

(A) Blue and red ovals represent nucleosomes along the *S. pombe ura4* and *his7* genes. Angles inside the ovals represent the +1N signature incorporated in the forward and reverse orientations into the nucleosomal DNA along the two genes. Bars below the genes indicate the 5′ and 3′ amplicons of each construct tested for RNA Pol II occupancy in (D). They do not overlap in the forward and reverse constructs because optimal sequences to place the primers are different in each case.

(B) Strand-specific expression of each construct in the forward and reverse orientation using total RNA as a template. Expression was normalized to the *S. pombe* actin *act1* gene.

(C) Expression of the same constructs using nascent RNA as a template (+ histograms). Values were normalized to the *ACT1* gene of *S. cerevisiae* as a spike-in control of nascent RNA. The − histograms indicate the level of transcription on RNA isolated without 4-thiouracil labeling. Values represent the average of two biological replicates.

(D) Active (Ser2-P) and total RNA Pol II occupancy measured by chromatin immunoprecipitation normalized as in Figure 3D. 5′ and 3′ in the x axis refer to the 5′ and 3′ amplicons of the four strains shown in (A). Histograms in (B) and (D) represent averages of three or four biological replicates per sample. Error bars indicate standard deviation.

(E) The +1N signature was incorporated into the forward and reverse orientations only in the first nucleosome of the *his7* gene (only +1N) or in the eight remaining nucleosomes downstream, while maintaining the wild-type version of +1N (not +1N).

(F) Expression of the four constructs in (E) using total RNA as a template. Expression was normalized as in (B).

(G) Expression of the same constructs using nascent RNA as a template (+ columns). Values were normalized to *S. cerevisiae* spike-in nascent RNA. + and − histograms are as in (C). Student's t test p values of all the comparisons are shown in Table S2.

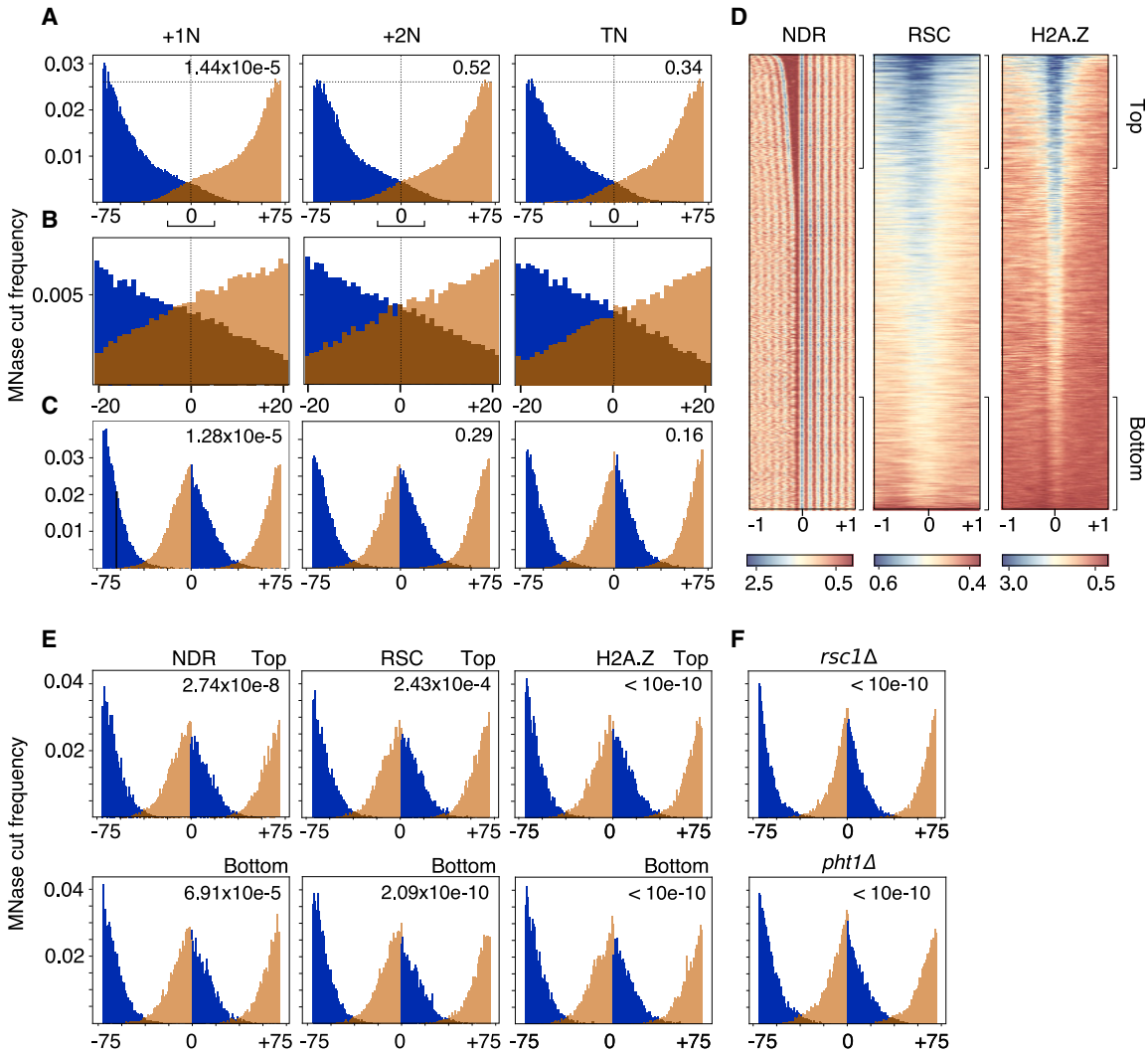

Figure 5. Asymmetrical accessibility of +1 nucleosomes to MNase

(A) Distribution of 5′ (blue) and 3′ (orange) ends of MNase fragments along nucleosomal DNA associated with +1N, +2N, and terminal (TN) groups of nucleosomes in Figure 1. Transcription proceeds from left to right. Vertical dotted lines indicate the dyad position in each group of nucleosomes. Differences in the symmetry of the distributions of 5′ and 3′ ends were estimated using the Kolmogorov-Smirnov (K-S) test (p values are indicated in each graph).

(B) The asymmetrical distribution of MNase cuts relative to the dyad region in +1N is also detectable in the expanded −20/+20 region indicated by brackets in (A).

(C) Distribution of 5′ and 3′ ends of fragments derived from the proximal (P) and distal (D) halves of the three groups of nucleosomes shown in (A) (K-S p values of the distribution of the 5′ ends of the proximal half and the 3′ ends of the distal half are indicated in each graph).

(D) *S. pombe* genes (4,474) aligned to the dyad of +1N and ranked according to the size of the 5′ NDR (NDR, red) or to the enrichment in RSC or H2A.Z (blue). Heatmaps represent genomic regions between −1 and +1 kb from the dyad of +1 nucleosomes (0).

(E) Distributions of 5′ and 3′ ends of fragments in the proximal and distal halves of +1 nucleosomes of the 1,000 top and bottom genes of the distributions indicated by brackets in (D).

(F) Same as (E) but in +1 nucleosomes of the *rsc1*Δ and *pht1*Δ mutants.

lacking H2A.Z and found that the MNase asymmetry of +1N was maintained as in wild-type cells (Figure 5F).

The signature of +1 nucleosomes specifies asymmetrical accessibility to MNase

Given the asymmetrical signature of +1 nucleosomes and the asymmetrical accessibility to MNase, we wondered whether both features would be functionally related. This possibility predicted that each of the nine nucleosomes that incorporated the +1N signature into the forward orientation along the *his7* gene in Figure 4A would mimic the asymmetrical accessibility to MNase found in +1 nucleosomes and that the pattern would be inverted in the reverse orientation. To test this, we sequenced subnucleosomal fragments from the two strains harboring the forward and reverse remastered *his7* gene in Figure 4A. Since the number of fragments aligning to each half of the nine individual nucleosomes along *his7* was small, the aggregated profile of MNase cuts along their proximal and distal halves (Figure 6A) was more noisy than in Figure 5C,

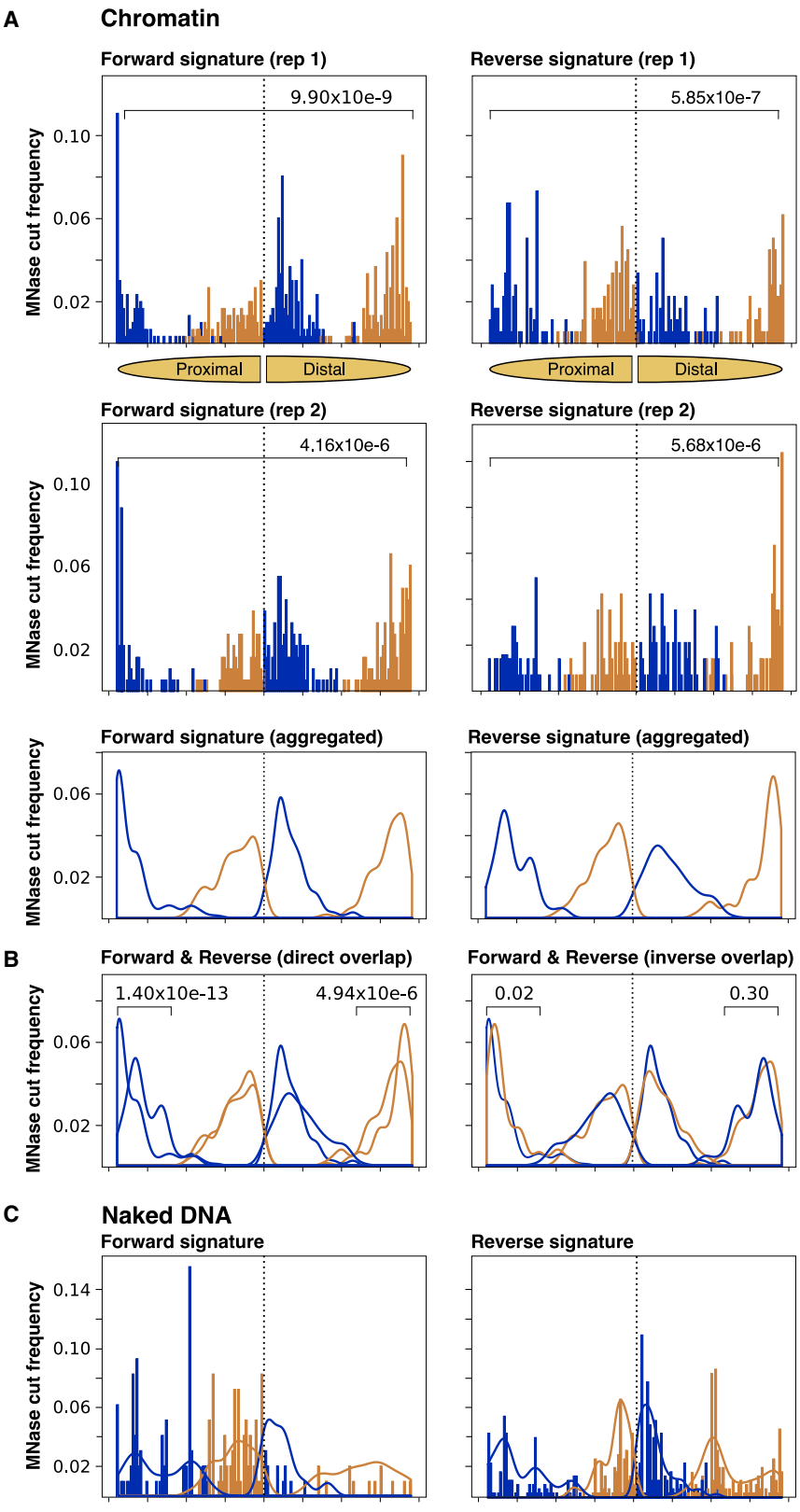

Figure 6. Nucleosomal signatures specify asymmetrical accessibility to MNase

(A) Aggregated distribution of 5′ (blue) and 3′ (orange) ends of MNase fragments in the proximal and distal halves of the nine nucleosomes along the *his7* gene that incorporated the +1N signature in the forward and reverse orientations in Figure 4A. In both cases, transcription proceeds from left to right. Results from two independent experiments are shown (rep 1 and rep 2) (K-S p values of the distribution of the 5′ end of the proximal and the 3′ end of the distal half in forward and reverse are indicated in each plot). Bottom shows the density plots of the aggregated distributions of 5′ and 3′ ends in rep 1 and rep 2.

(B) Direct and inverse overlap of the forward and reverse density plots shown in (A) (K-S p values of the differences in the distribution of the 5′ and 3′ ends of the proximal and distal halves in the direct and inverse overlap are indicated in each plot).

(C) Distributions of 5′ and 3′ ends in naked DNA in the same genome regions shown in (A).

where it was derived from thousands of nucleosomes. However, results from two independent experiments showed that the profile of MNase cuts along the nine nucleosomes incorporating the +1N signature in the forward orientation mimicked the profile of +1N in the genome (Figure 6A, left). Crucially, this pattern was inverted in the same nucleosomes along the *his7* gene in the strain that incorporated the reverse +1N signature (Figure 6A, right). This is clearly shown by the close overlap of the density profiles of the forward and the mirror image of the reverse distribution (Figure 6B, inverse overlap). Naked DNA controls of the same nine nucleosomes showed that the pattern of MNase cuts in chromatin was not due to a sequence bias of the MNase (Figure 6C). Altogether, these results support that the asymmetrical DNA signature of a +1 nucleosome by itself can confer asymmetrical accessibility to MNase when incorporated into nucleosomes along the transcribed region of the *his7* gene.

DISCUSSION

There is increasing evidence from *in vitro* studies that nucleosomes can display asymmetrical properties specified by different sequence elements distributed along nucleosomal DNA.[22,25,28–30,32] During transcription, RNA polymerase pauses preferentially at specific locations coinciding with sites of stronger DNA-histone interaction. Current models propose that pausing is required to form an intranucleosomal DNA loop upstream of the dyad that could act as a histone transfer intermediate to maintain the nucleosome position relative to the DNA sequence. According to these studies, pausing would be favored by sequences in the distal half of the nucleosomal DNA that retain the nucleosome to prevent its eviction while the RNA polymerase peels off the DNA from the proximal half.[29,31,33,34,41]

In line with these observations, we have found that the two halves of nucleosomal DNA contribute differentially to the stability of nucleosomes *in vivo*, such that modifying the distal half of the *S. pombe ura4* and *his7* nucleosomes disrupts their organization and reduces the expression of both genes. By contrast, changes in the proximal half have a negligible effect, both in the nucleosomal profile and in expression, suggesting that sequence elements in the distal half are more critical for nucleosome stability (Figures 2A, S5, and S6). This functional complementarity between the two halves of nucleosomal DNA seems to be a general property of nucleosomes, since chimeric DNA fragments made by linking the proximal and distal halves of unrelated nucleosomes reconstitute the same periodic pattern as the endogenous sequences (Figure 2B).

It is interesting that disruption of +1N in the *ura4* gene does not affect the position of nucleosomes downstream (Figure 2A), consistent with our previous findings.[36] This contrasts with the expectations of the statistical positioning model[54] that proposes that +1N, in combination with transcription factors and ATP-dependent chromatin remodelers, acts as a barrier from where downstream nucleosomes are positioned, as supported by *in vitro* experiments on reconstituted chromatin in *S. cerevisiae*.[55,56] Our results suggest that the contribution of the +1N to positioning adjacent nucleosomes is different in *S. pombe* and in *S. cerevisiae*. This could be due to differences between the two yeasts in the organization of promoters, the average spacing between nucleosomes,[50] or the presence of linker histone H1 in *S. cerevisiae*. Alternatively, the contribution of +1N to statistical positioning could be less relevant *in vivo* than *in vitro*.

The importance of the orientation of nucleosomal DNA to modulate transcription directionality is highlighted by the different permissiveness along constructs made up of +1 nucleosomal DNA in the forward and reverse orientations (Figure 3). Antisense control is important in the compact genome of *S. pombe*, where the average gene density is one every 2–2.5 kb and where many promoters are inherently bidirectional.[46,57] In this yeast, transcriptional termination is not as efficient and sharply defined as in *S. cerevisiae*, and the RNA polymerase tends to reach a variable distance downstream of the cleavage polyadenylation signal.[37,46,58–60] Consequently, antisense transcription has been detected in 70% of all *S. pombe* protein-coding genes and correlates with downregulation of sense transcription.[46,57] It is likely that antisense transcription along the reverse modified *ura4* and *his7* genes (Figures 4B and 4C) derives from defective termination of the convergent downstream genes *tam14* and *ccc2*, respectively. The higher level of antisense in the reverse modified *ura4* gene is consistent with Native Elongating Transcript sequencing (NET-seq) experiments showing that active polymerases from *tam14* reach half way up the convergent *ura4* gene, while in *ccc2* they only overlap the 3′ end of the *his7* gene.[46] It also correlates with a higher ratio of antisense/sense in the wild-type *ura4* than in the *his7* genes (Figure S5C).

Although in many organisms some antisense transcripts have a regulatory role,[61] a possible threat is that transcription over NDRs at promoters could cause their inactivation by removal of transcription factors or by unscheduled nucleosome occupancy through reduced binding of the RSC chromatin remodeler by deacetylation of the +1 and −1 nucleosomes.[62,63] The strong opposition of +1N to antisense transcription could protect promoters from such an eventuality.

The contribution of nucleosomes downstream of +1N to transcription directionality is not significant under the same conditions used to analyze +1N, since only one of the two constructs made up of central nucleosomes along genes (CN-A) showed a small decrease in transcription in the reverse orientation in total RNA (Figure 3B). The signature of these nucleosomes, however, is not as strongly asymmetrical as that of +1N (Figure 1A), and it is possible that their input to transcription directionality could vary depending on the sequence constraints imposed in individual nucleosomal DNAs to encode a functional protein. The minor contribution of downstream nucleosomes relative to +1N is also illustrated by the results in Figures 4F and 4G. However, a collective, albeit minor, contribution could still be significant based on *in vitro* experiments showing that the unwrapping of the two ends of nucleosomal DNA is coordinated such that even a relatively small asymmetry between the two sides can be amplified to generate a large asymmetry in the mechanical stability of the entire nucleosome.[22]

Asymmetrical accessibility of MNase to the region between the −6 and the +6 positions flanking the dyad of +1 nucleosomes has been reported in *S. cerevisiae*.[51] In that case, asymmetrical nucleosomes were enriched in the RSC remodeler and the H2A.Z histone variant. In *S. pombe*, however, asymmetrical accessibility of +1N is independent of RSC and H2AZ (Figures 5E and 5F).

It is possible that the accumulation of RNA Pol II in the proximal half of the +1 nucleosome (Figure 1B) or the proximity to transcription factors bound to the promoter could partially contribute to the asymmetrical accessibility to MNase in *S. pombe* chromatin. However, the relevance of the DNA sequence is supported by the fact that the same asymmetry is detected in non-+1 nucleosomes along the *his7* gene after incorporating the +1N signature along their length (Figure 6A). Crucially, the asymmetry follows a mirror image profile depending on the orientation of the signature (Figure 6B), suggesting that these properties depend on the different affinity of each half of nucleosomal DNA for the histone core. Very relevant to these results, a recent genome-wide analysis of DNA cyclizability as a measure of bendability of nucleosomal DNA in *S. cerevisiae* showed that cyclizability differs not only between +1N and downstream nucleosomes but also between the two halves of +1N. In addition, substitution of wild-type codons by synonymous codons alters the potential for cyclizability.[27] These observations are consistent with the differential contribution of each half of nucleosomal DNA to nucleosome stability (Figure 2) and with our previous report that replacement of the wild-type codons by synonymous codons completely deranges nucleosome stability.[36]

Altogether, our results show that asymmetrical signatures contain information to endow nucleosomes with asymmetrical properties that modulate transcription directionality. This implies that nucleosomal DNA has the potential to encode overlapping layers of information[64] that could include, for example, the asymmetric GC-rich elements in *S. cerevisiae* +1 nucleosomes that specify the order in which the Swi2/Snf2-related 1 (SWR1) remodeling complex replaces each H2A-H2B with an H2A.Z-H2B dimer.[65]

Limitations of the study

A limitation of functional analyses *in vivo* is the number of cases that can be analyzed. We have tested eight constructs in the forward and reverse orientations, each made up of eight individual +1 or central nucleosomal DNAs from genes selected at random in the genome (Figure 3). Since each fragment has a different sequence, we would expect some variation in the efficiency of transcription along different constructs. Some examples of the variability in the shape and pattern of occupancy among individual wild-type nucleosomes are shown in Figures S2 and S4. It is possible that the impact of transcription results from the cumulative contribution of each nucleosomal fragment. The same limitation applies to the eight constructs in Figure 4. In this case, incorporation of the +1N signature in the two orientations along the *ura4* and *his7* genes will show some variation between nucleosomes depending on the coding constraints imposed by the codons of the two genes. Despite these limitations, results are consistent in all the cases that we have analyzed and show that the forward or reverse orientation of nucleosomal DNA allows or hinders transcription and modulates the balance between sense and antisense transcription.

STAR★METHODS

Detailed methods are provided in the online version of this paper and include the following:

- KEY RESOURCES TABLE
- RESOURCE AVAILABILITY
  - Lead contact
  - Materials availability
  - Data and code availability
- EXPERIMENTAL MODEL AND STUDY PARTICIPANT DETAILS
  - Yeast strains
- METHOD DETAILS
  - Growth conditions and construction of *S. pombe* strains harbouring modified DNA sequences
  - Preparation of mononucleosomal and subnucleosomal DNA fragments and naked DNA controls
  - Alignment of sequence reads and DANPOS analysis
  - Chromatin immunoprecipitation and qPCR
  - RNA isolation, RT-qPCR and transcript stability
  - RNA labeling and newly transcribed RNA purification
- QUANTIFICATION AND STATISTICAL ANALYSIS
  - Identification of nucleosome groups along transcription units
  - Generation of nucleotide profiles along nucleosomal DNA
  - Statistical analysis
  - Incorporation of nucleosomal signatures in the *his7* and *ura4* ORFs sequences by codon substitution

SUPPLEMENTAL INFORMATION

Supplemental information can be found online at https://doi.org/10.1016/j.celrep.2023.113605.

ACKNOWLEDGMENTS

We are grateful to Félix Prado and José Carlos Reyes (CABIMER, Sevilla) for helpful comments on the manuscript and to José Manuel Santos (Departamento de Estadística, Universidad de Salamanca) for advice on the statistical analyses. This work was funded by grant PID2020-118423GB-I00 funded by MCIN/AEI/10.13039/501100011033.

AUTHOR CONTRIBUTIONS

A.G. performed genetic and biochemical experiments and bioinformatic and DANPOS analyses. L.D. carried out the bioinformatic and statistical analyses of the MNase-seq experiments and contributed to transcription analyses. S.G. contributed to the construction of strains and to MNase and transcription analyses. M.S. performed genetic and biochemical experiments and the genomic sequencing. R.S. carried out computational analyses and wrote the script to incorporate signatures into nucleosomal DNA. F.A. supervised the general strategy of the work, analyzed data, and wrote the manuscript. All authors contributed to the designing of the experiments, analyzed data, and approved the final version of the manuscript.

DECLARATION OF INTERESTS

The authors declare no competing interests.

Received: February 16, 2023
Revised: October 3, 2023
Accepted: December 5, 2023

REFERENCES

1. Washietl, S., Machné, R., and Goldman, N. (2008). Evolutionary footprints of nucleosome positions in yeast. Trends Genet. *24*, 583–587.
2. Warnecke, T., Batada, N.N., and Hurst, L.D. (2008). The impact of the nucleosome code on protein-coding sequence evolution in yeast. PLoS Genet. *4*, e1000250.
3. Langley, S.A., Karpen, G.H., and Langley, C.H. (2014). Nucleosomes shape DNA polymorphism and divergence. PLoS Genet. *10*, e1004457.
4. Li, Y., Li, C., Li, S., Peng, Q., An, N.A., He, A., and Li, C.Y. (2018). Human exonization through differential nucleosome occupancy. Proc. Natl. Acad. Sci. USA *115*, 8817–8822.
5. Clapier, C.R., Iwasa, J., Cairns, B.R., and Peterson, C.L. (2017). Mechanisms of action and regulation of ATP-dependent chromatin-remodelling complexes. Nat. Rev. Mol. Cell Biol. *18*, 407–422.
6. Reyes, A.A., Marcum, R.D., and He, Y. (2021). Structure and Function of Chromatin Remodelers. J. Mol. Biol. *433*, 166929.
7. Whitehouse, I., Rando, O.J., Delrow, J., and Tsukiyama, T. (2007). Chromatin remodelling at promoters suppresses antisense transcription. Nature *450*, 1031–1035.
8. Shim, Y.S., Choi, Y., Kang, K., Cho, K., Oh, S., Lee, J., Grewal, S.I.S., and Lee, D. (2012). Hrp3 controls nucleosome positioning to suppress non-coding transcription in eu- and heterochromatin. EMBO J. *31*, 4375–4387.
9. Kubik, S., Bruzzone, M.J., Challal, D., Dreos, R., Mattarocci, S., Bucher, P., Libri, D., and Shore, D. (2019). Opposing chromatin remodelers control transcription initiation frequency and start site selection. Nat. Struct. Mol. Biol. *26*, 744–754.
10. Marquardt, S., Escalante-Chong, R., Pho, N., Wang, J., Churchman, L.S., Springer, M., and Buratowski, S. (2014). A chromatin-based mechanism for limiting divergent noncoding transcription. Cell *157*, 1712–1723.
11. Hainer, S.J., Gu, W., Carone, B.R., Landry, B.D., Rando, O.J., Mello, C.C., and Fazzio, T.G. (2015). Suppression of pervasive noncoding transcription in embryonic stem cells by esBAF. Genes Dev. *29*, 362–378.
12. Alcid, E.A., and Tsukiyama, T. (2014). ATP-dependent chromatin remodeling shapes the long noncoding RNA landscape. Genes Dev. *28*, 2348–2360.
13. Kaplan, C.D., Laprade, L., and Winston, F. (2003). Transcription elongation factors repress transcription initiation from cryptic sites. Science *301*, 1096–1099.
14. Becker, P.B., and Workman, J.L. (2013). Nucleosome remodeling and epigenetics. Cold Spring Harb. Perspect. Biol. *5*, a017905.
15. Pardal, A.J., Fernandes-Duarte, F., and Bowman, A.J. (2019). The histone chaperoning pathway: from ribosome to nucleosome. Essays Biochem. *63*, 29–43.
16. Martire, S., and Banaszynski, L.A. (2020). The roles of histone variants in fine-tuning chromatin organization and function. Nat. Rev. Mol. Cell Biol. *21*, 522–541.
17. Zhou, K., Liu, Y., and Luger, K. (2020). Histone chaperone FACT FAcilitates Chromatin Transcription: mechanistic and structural insights. Curr. Opin. Struct. Biol. *65*, 26–32.
18. Luger, K., Rechsteiner, T.J., Flaus, A.J., Waye, M.M., and Richmond, T.J. (1997). Characterization of nucleosome core particles containing histone proteins made in bacteria. J. Mol. Biol. *272*, 301–311.
19. Chua, E.Y.D., Vasudevan, D., Davey, G.E., Wu, B., and Davey, C.A. (2012). The mechanics behind DNA sequence-dependent properties of the nucleosome. Nucleic Acids Res. *40*, 6338–6352.
20. Thåström, A., Lowary, P.T., Widlund, H.R., Cao, H., Kubista, M., and Widom, J. (1999). Sequence motifs and free energies of selected natural and non-natural nucleosome positioning DNA sequences. J. Mol. Biol. *288*, 213–229.
21. Arimura, Y., Shih, R.M., Froom, R., and Funabiki, H. (2021). Structural features of nucleosomes in interphase and metaphase chromosomes. Mol. Cell *81*, 4377–4397.e12.
22. Ngo, T.T.M., Zhang, Q., Zhou, R., Yodh, J.G., and Ha, T. (2015). Asymmetric unwrapping of nucleosomes under tension directed by DNA local flexibility. Cell *160*, 1135–1144.
23. de Bruin, L., Tompitak, M., Eslami-Mossallam, B., and Schiessel, H. (2016). Why Do Nucleosomes Unwrap Asymmetrically? J. Phys. Chem. B *120*, 5855–5863.
24. Chen, Y., Tokuda, J.M., Topping, T., Meisburger, S.P., Pabit, S.A., Gloss, L.M., and Pollack, L. (2017). Asymmetric unwrapping of nucleosomal DNA propagates asymmetric opening and dissociation of the histone core. Proc. Natl. Acad. Sci. USA *114*, 334–339.
25. Mauney, A.W., Tokuda, J.M., Gloss, L.M., Gonzalez, O., and Pollack, L. (2018). Local DNA Sequence Controls Asymmetry of DNA Unwrapping from Nucleosome Core Particles. Biophys. J. *115*, 773–781.
26. Onufriev, A.V., and Schiessel, H. (2019). The nucleosome: from structure to function through physics. Curr. Opin. Struct. Biol. *56*, 119–130.
27. Basu, A., Bobrovnikov, D.G., Qureshi, Z., Kayikcioglu, T., Ngo, T.T.M., Ranjan, A., Eustermann, S., Cieza, B., Morgan, M.T., Hejna, M., et al. (2021). Measuring DNA mechanics on the genome scale. Nature *589*, 462–467.
28. Bondarenko, V.A., Steele, L.M., Ujvári, A., Gaykalova, D.A., Kulaeva, O.I., Polikanov, Y.S., Luse, D.S., and Studitsky, V.M. (2006). Nucleosomes can form a polar barrier to transcript elongation by RNA polymerase II. Mol. Cell *24*, 469–479.
29. Kulaeva, O.I., Gaykalova, D.A., Pestov, N.A., Golovastov, V.V., Vassylyev, D.G., Artsimovitch, I., and Studitsky, V.M. (2009). Mechanism of chromatin remodeling and recovery during passage of RNA polymerase II. Nat. Struct. Mol. Biol. *16*, 1272–1278.
30. Gaykalova, D.A., Kulaeva, O.I., Volokh, O., Shaytan, A.K., Hsieh, F.K., Kirpichnikov, M.P., Sokolova, O.S., and Studitsky, V.M. (2015). Structural analysis of nucleosomal barrier to transcription. Proc. Natl. Acad. Sci. USA *112*, 5787–5795.
31. Kujirai, T., Ehara, H., Fujino, Y., Shirouzu, M., Sekine, S.I., and Kurumizaka, H. (2018). Structural basis of the nucleosome transition during RNA polymerase II passage. Science *362*, 595–598.
32. Noe Gonzalez, M., Blears, D., and Svejstrup, J.Q. (2021). Causes and consequences of RNA polymerase II stalling during transcript elongation. Nat. Rev. Mol. Cell Biol. *22*, 3–21.
33. Kujirai, T., and Kurumizaka, H. (2020). Transcription through the nucleosome. Curr. Opin. Struct. Biol. *61*, 42–49.
34. Filipovski, M., Soffers, J.H.M., Vos, S.M., and Farnung, L. (2022). Structural basis of nucleosome retention during transcription elongation. Science *376*, 1313–1316.
35. Quintales, L., Soriano, I., Vázquez, E., Segurado, M., and Antequera, F. (2015). A species-specific nucleosomal signature defines a periodic distribution of amino acids in proteins. Open Biol. *5*, 140218.
36. González, S., García, A., Vázquez, E., Serrano, R., Sánchez, M., Quintales, L., and Antequera, F. (2016). Nucleosomal signatures impose nucleosome positioning in coding and noncoding sequences in the genome. Genome Res. *26*, 1532–1543.
37. Booth, G.T., Wang, I.X., Cheung, V.G., and Lis, J.T. (2016). Divergence of a conserved elongation factor and transcription regulation in budding and fission yeast. Genome Res. *26*, 799–811.
38. Ehara, H., Kujirai, T., Fujino, Y., Shirouzu, M., Kurumizaka, H., and Sekine, S.I. (2019). Structural insight into nucleosome transcription by RNA polymerase II with elongation factors. Science *363*, 744–747.
39. Chen, Z., Gabizon, R., Brown, A.I., Lee, A., Song, A., Díaz-Celis, C., Kaplan, C.D., Koslover, E.F., Yao, T., and Bustamante, C. (2019). High-resolution and high-accuracy topographic and transcriptional maps of the nucleosome barrier. Elife *8*, e48281.

40. Churchman, L.S., and Weissman, J.S. (2011). Nascent transcript sequencing visualizes transcription at nucleotide resolution. Nature *469*, 368–373.

41. Kulaeva, O.I., Hsieh, F.K., Chang, H.W., Luse, D.S., and Studitsky, V.M. (2013). Mechanism of transcription through a nucleosome by RNA polymerase II. Biochim. Biophys. Acta *1829*, 76–83.

42. Chen, K., Xi, Y., Pan, X., Li, Z., Kaestner, K., Tyler, J., Dent, S., He, X., and Li, W. (2013). DANPOS: dynamic analysis of nucleosome position and occupancy by sequencing. Genome Res. *23*, 341–351.

43. Soriano, I., Quintales, L., and Antequera, F. (2013). Clustered regulatory elements at nucleosome-depleted regions punctuate a constant nucleosomal landscape in *Schizosaccharomyces pombe*. BMC Genom. *14*, 813.

44. Pelechano, V., and Pérez-Ortín, J.E. (2008). The transcriptional inhibitor thiolutin blocks mRNA degradation in yeast. Yeast *25*, 85–92.

45. Baptista, T., and Devys, D. (2018). Saccharomyces cerevisiae Metabolic Labeling with 4-thiouracil and the Quantification of Newly Synthesized mRNA As a Proxy for RNA Polymerase II Activity. J. Vis. Exp. *140*, e57982.

46. Wery, M., Gautier, C., Descrimes, M., Yoda, M., Vennin-Rendos, H., Migeot, V., Gautheret, D., Hermand, D., and Morillon, A. (2018). Native elongating transcript sequencing reveals global anti-correlation between sense and antisense nascent transcription in fission yeast. RNA *24*, 196–208.

47. Lauinger, L., Li, J., Shostak, A., Cemel, I.A., Ha, N., Zhang, Y., Merkl, P.E., Obermeyer, S., Stankovic-Valentin, N., Schafmeier, T., et al. (2017). Thiolutin is a zinc chelator that inhibits the Rpn11 and other JAMM metalloproteases. Nat. Chem. Biol. *13*, 709–714.

48. Kim, M.J., Kim, M., and Park, S.D. (2002). Post-transcriptional regulation of *ura4+* gene expression by glucose in *Schizosaccharomyces pombe*. Mol. Cells *14*, 437–443. https://www.molcells.org/journal/view.html?year=2002&volume=14&number=3&spage=437.

49. Henikoff, J.G., Belsky, J.A., Krassovsky, K., MacAlpine, D.M., and Henikoff, S. (2011). Epigenome characterization at single base-pair resolution. Proc. Natl. Acad. Sci. USA *108*, 18318–18323.

50. Lantermann, A.B., Straub, T., Strålfors, A., Yuan, G.C., Ekwall, K., and Korber, P. (2010). Schizosaccharomyces pombe genome-wide nucleosome mapping reveals positioning mechanisms distinct from those of *Saccharomyces cerevisiae*. Nat. Struct. Mol. Biol. *17*, 251–257.

51. Ramachandran, S., Zentner, G.E., and Henikoff, S. (2015). Asymmetric nucleosomes flank promoters in the budding yeast genome. Genome Res. *25*, 381–390.

52. Lee, J., Choi, E.S., Seo, H.D., Kang, K., Gilmore, J.M., Florens, L., Washburn, M.P., Choe, J., Workman, J.L., and Lee, D. (2017). Chromatin remodeller Fun30(Fft3) induces nucleosome disassembly to facilitate RNA polymerase II elongation. Nat. Commun. *8*, 14527.

53. Clément-Ziza, M., Marsellach, F.X., Codlin, S., Papadakis, M.A., Reinhardt, S., Rodríguez-López, M., Martin, S., Marguerat, S., Schmidt, A., Lee, E., et al. (2014). Natural genetic variation impacts expression levels of coding, non-coding, and antisense transcripts in fission yeast. Mol. Syst. Biol. *10*, 764.

54. Kornberg, R.D., and Stryer, L. (1988). Statistical distributions of nucleosomes: nonrandom locations by a stochastic mechanism. Nucleic Acids Res. *16*, 6677–6690.

55. Zhang, Z., Wippo, C.J., Wal, M., Ward, E., Korber, P., and Pugh, B.F. (2011). A packing mechanism for nucleosome organization reconstituted across a eukaryotic genome. Science *332*, 977–980.

56. Krietenstein, N., Wal, M., Watanabe, S., Park, B., Peterson, C.L., Pugh, B.F., and Korber, P. (2016). Genomic Nucleosome Organization Reconstituted with Pure Proteins. Cell *167*, 709–721.e12.

57. Atkinson, S.R., Marguerat, S., Bitton, D.A., Rodríguez-López, M., Rallis, C., Lemay, J.F., Cotobal, C., Malecki, M., Smialowski, P., Mata, J., et al. (2018). Long noncoding RNA repertoire and targeting by nuclear exosome, cytoplasmic exonuclease, and RNAi in fission yeast. RNA *24*, 1195–1213.

58. Gullerova, M., and Proudfoot, N.J. (2008). Cohesin complex promotes transcriptional termination between convergent genes in *S. pombe*. Cell *132*, 983–995.

59. Mata, J. (2013). Genome-wide mapping of polyadenylation sites in fission yeast reveals widespread alternative polyadenylation. RNA Biol. *10*, 1407–1414.

60. Liu, X., Hoque, M., Larochelle, M., Lemay, J.F., Yurko, N., Manley, J.L., Bachand, F., and Tian, B. (2017). Comparative analysis of alternative polyadenylation in *S. cerevisiae* and *S. pombe*. Genome Res. *27*, 1685–1695.

61. Mellor, J., Woloszczuk, R., and Howe, F.S. (2016). The interleaved genome. Trends Genet. *32*, 57–71.

62. Dai, Z., and Dai, X. (2012). Antisense transcription is coupled to nucleosome occupancy in sense promoters. Bioinformatics *28*, 2719–2723.

63. Gill, J.K., Maffioletti, A., García-Molinero, V., Stutz, F., and Soudet, J. (2020). Fine Chromatin-Driven Mechanism of Transcription Interference by Antisense Noncoding Transcription. Cell Rep. *31*, 107612.

64. Eslami-Mossallam, B., Schram, R.D., Tompitak, M., van Noort, J., and Schiessel, H. (2016). Multiplexing Genetic and Nucleosome Positioning Codes: A Computational Approach. PLoS One *11*, e0156905.

65. Sun, L., Pierrakeas, L., Li, T., and Luk, E. (2020). Thermosensitive Nucleosome Editing Reveals the Role of DNA Sequence in Targeted Histone Variant Deposition. Cell Rep. *30*, 257–268.e5.

66. Keifenheim, D., Sun, X.M., D'Souza, E., Ohira, M.J., Magner, M., Mayhew, M.B., Marguerat, S., and Rhind, N. (2017). Size-Dependent Expression of the Mitotic Activator Cdc25 Suggests a Mechanism of Size Control in Fission Yeast. Curr. Biol. *27*, 1491–1497.e4.

67. Langmead, B., Trapnell, C., Pop, M., and Salzberg, S.L. (2009). Ultrafast and memory-efficient alignment of short DNA sequences to the human genome. Genome Biol. *10*, R25.

68. Quinlan, A.R., and Hall, I.M. (2010). BEDTools: a flexible suite of utilities for comparing genomic features. Bioinformatics *26*, 841–842.

69. Quintales, L., Vázquez, E., and Antequera, F. (2015). Comparative analysis of methods for genome-wide nucleosome cartography. Brief. Bioinform. *16*, 576–587.

70. Ramírez, F., Ryan, D.P., Grüning, B., Bhardwaj, V., Kilpert, F., Richter, A.S., Heyne, S., Dündar, F., and Manke, T. (2016). deepTools2: a next generation web server for deep-sequencing data analysis. Nucleic Acids Res. *44*, W160–W165.

71. Hunter, J.D. (2007). Matplotlib: A 2D Graphics Environment. Comput. Sci. Eng. *9*, 90–95.

72. Waskom, M. (2021). Seaborn: statistical data visualization. J. Open Source Softw. *6*, 3021.

73. Moreno, S., Klar, A., and Nurse, P. (1991). Molecular genetic analysis of fission yeast *Schizosaccharomyces pombe*. Methods Enzymol. *194*, 795–823.

74. Rodríguez-López, M., Cotobal, C., Fernández-Sánchez, O., Borbarán Bravo, N., Oktriani, R., Abendroth, H., Uka, D., Hoti, M., Wang, J., Zaratiegui, M., and Bähler, J. (2017). A CRISPR/Cas9-based method and primer design tool for seamless genome editing in fission yeast. Wellcome Open Res. *1*, 19.

75. Pidoux, A., Mellone, B., and Allshire, R. (2004). Analysis of chromatin in fission yeast. Methods *33*, 252–259.

76. Li, H., Hou, J., Bai, L., Hu, C., Tong, P., Kang, Y., Zhao, X., and Shao, Z. (2015). Genome-wide analysis of core promoter structures in *Schizosaccharomyces pombe* with DeepCAGE. RNA Biol. *12*, 525–537.

77. Nagalakshmi, U., Wang, Z., Waern, K., Shou, C., Raha, D., Gerstein, M., and Snyder, M. (2008). The transcriptional landscape of the yeast genome defined by RNA sequencing. Science *320*, 1344–1349.

78. Rhind, N., Chen, Z., Yassour, M., Thompson, D.A., Haas, B.J., Habib, N., Wapinski, I., Roy, S., Lin, M.F., Heiman, D.I., et al. (2011). Comparative functional genomics of the fission yeasts. Science *332*, 930–936.

STAR★METHODS

KEY RESOURCES TABLE

REAGENT or RESOURCE	SOURCE	IDENTIFIER
Antibodies		
RNA polymerase II CTD repeat YSPTSPS antibody	Abcam	ab26721 (RRID: AB_777726)
Anti-RNA polymerase II CTD repeat YSPTSPS (phospho S2) antibody	Abcam	ab5095 (RRID: AB_304749)
Chemicals, peptides, and recombinant proteins		
Zymolyase (R) 20T (Arthrobacter luteus)	Amsbio	120491-1
Nuclease micrococcal from Staphylococcus aureus	Thermo Scientific™	EN0181
Proteinase K	Roche	3115879001
Complete™ Protease Inhibitor Cocktail	Roche	11697498001
Phosphatase Inhibitor Cocktail PhosSTOP™	Roche	4906845001
Dynabeads Protein G for Immunoprecipitation	Invitrogen™	10003D
Thiolutin	Abcam	ab143556
4-Thiouracil	Sigma-Aldrich	440736
EZ-Link HPDP-Biotin, No-Weigh Format	Thermo Scientific™	21341
Formaldehyde solution 36,5-38%	Sigma-Aldrich	F8775
RNase A from bovine pancreas	Roche	10109142001
Phenol equilibrated, stabilized : Chloroform : Isoamyl Alcohol 25 : 24 : 1	PanReacAppliChem	A0889
ß-Mercaptoethanol	Sigma-Aldrich	M6250
Phire Green Hot Start II PCR Master Mix	Thermo Scientific™	F126S
Phusion Green Hot Start II High-Fidelity DNA Polymerase	Thermo Scientific™	F537S
5-Fluoro Orotic Acid Monohidrate	Apollo Scientific	PC4054
G-418 Disulphate	Gibco™	11811023
Critical commercial assays		
RNeasy Mini Kit (50)	Qiagen	74104
NZY Total RNA Isolation kit	NZYTech	MB13402
µMACS™ Streptavidin Kit	Miltenyi Biotec	130-074-101
TB Green® Premix Ex Taq™ (Tli RNase H Plus)	Takara	RR420A
Biotools High Retrotrasncriptase Starter Kit with Oligo dT and random primers	Biotools	10082-4119
Blood & Cell Culture DNA Midi Kit	Qiagen	13343
GFX PCR DNA and gel band purification kit	Cytiva	10536295
Freeze 'N Sequeeze DNA Gel Extraction Spin Columns	Biorad	7326165
Qubit dsDNA HS Kit, 500	Invitrogen™	Q32854
Qubit Assay tubes, 500	Invitrogen™	Q32856
High Sensitivity DNA Kit	Agilent	5067–4626
Sera-Mag Select DNA size selection and PCR Clean-Up kit	Cytiva	29343052
PhiX v3 control	Illumina	FC-110-3001
Nextera XT index kit 24 index, 96 samples	Perkin-Elmer	820037
NEXTFLEX ChIP-Seq kit 48 rxns	Perkin-Elmer	820020
NextSeq® 500 High Output v2.5 Kit (75 cycles)	Illumina	20024906

(*Continued on next page*)

Continued

REAGENT or RESOURCE	SOURCE	IDENTIFIER
Deposited data		
Sequence Read Archive (SRA)	https://www.ncbi.nlm.nih.gov/bioproject/PRJNA929707	PRJNA929707
Experimental Models: Organisms/Strains		
Strains used in this work are listed in Table S3	Table S3	N/A
Oligonucleotides		
Oligonucleotides are listed in Table S4	Sigma-Aldrich	N/A
Recombinant DNA		
ura4_Proximal(+1N)	gBlocks™ Gene Fragments IDT	Custom DNA
ura4_Distal	gBlocks™ Gene Fragments IDT	Custom DNA
ura4_Proximal	gBlocks™ Gene Fragments IDT	Custom DNA
his7_Distal	gBlocks™ Gene Fragments IDT	Custom DNA
his7_Proximal	gBlocks™ Gene Fragments IDT	Custom DNA
Complementary	gBlocks™ Gene Fragments IDT	Custom DNA
Codirectional	gBlocks™ Gene Fragments IDT	Custom DNA
+1N-A	gBlocks™ Gene Fragments IDT	Custom DNA
+1N-B	gBlocks™ Gene Fragments IDT	Custom DNA
CN-A	gBlocks™ Gene Fragments IDT	Custom DNA
CN-B	gBlocks™ Gene Fragments IDT	Custom DNA
ura4_for	gBlocks™ Gene Fragments IDT	Custom DNA
ura4_rev	gBlocks™ Gene Fragments IDT	Custom DNA
his7_for	gBlocks™ Gene Fragments IDT	Custom DNA
his7_rev	gBlocks™ Gene Fragments IDT	Custom DNA
his7_Only+1N	gBlocks™ Gene Fragments IDT	Custom DNA
his7_Not+1N	gBlocks™ Gene Fragments IDT	Custom DNA
Software and algorithms		
Bowtie	Langmead et al.[67]	http://bowtie-bio.sourceforge.net/index.shtml
Bedtools	Quinlan and Hall[68]	https://bedtools.readthedocs.io/en/latest/
Nucwave	Quintales et al.[69]	http://nucleosome.usal.es/nucwave
DANPOS	Chen et al.[42]	https://sites.google.com/site/danposdoc/home?authuser=0
deepTools	Ramírez et al.[70]	https://deeptools.readthedocs.io/en/develop/index.html
Matplotlib	Hunter[71]	https://matplotlib.org
Seaborn	Waskom[72]	https://seaborn.pydata.org/index.html
remaster.py	This work	https://github.com/rodrigoSantamaria/remaster

RESOURCE AVAILABILITY

Lead contact

Further information and requests for resources and reagents should be directed to and will be fulfilled by the lead contact, Francisco Antequera (cpg@usal.es).

Materials availability

Yeast strains generated in this study (Figure S3) are available upon request to the lead contact.

Data and code availability

- All genomic sequencing data generated for this work have been submitted to the NCBI Sequence Read Archive (SRA) and are publicly accessible under accession number PRJNA929707. (https://www.ncbi.nlm.nih.gov/bioproject/PRJNA929707).
- Code to incorporate nucleosomal signatures into DNA sequences is freely available at GitHub under a GPL 3.0 License (https://github.com/rodrigoSantamaria/remaster).

- Any additional information required to reanalyze the data reported in this work paper is available from the lead contact upon request.

EXPERIMENTAL MODEL AND STUDY PARTICIPANT DETAILS

Yeast strains

Yeast strains used in this work are listed in Table S3.

METHOD DETAILS

Growth conditions and construction of *S. pombe* strains harbouring modified DNA sequences

Schizosaccharomyces pombe h-, *h- leu 1-32 ura4 DS-E* (harbouring an internal deletion of the *ura4* ORF), *h- ura4-d18* and *S. pombe* 972 *h+ ade6-M210 leu1-32 ura4-d18* strains were grown at 32 ºC in rich medium[73]. All customized DNA molecules used in this work were synthesized by gBlocks® Gene Fragments (Integrated DNA Technologies). Modified versions of the *ura4* gene flanked by recombination cassettes 100–150 bp long were transformed into the *S. pombe ura4 DS-E* strain by electroporation and transformant colonies were selected on plates of minimal medium[73]. To construct the distal/proximal *his7* strains in Figure 2, the endogenous *his7* wild type gene was replaced by the *ura4* gene in an *ura4- S. pombe* d18 strain and transformants were selected in minimal medium. The *ura4* gene was subsequently replaced by the distal/proximal versions of the *his7* gene and transformants were selected on plates of minimal medium containing 1 mg/ml 5-fluoroorotic acid (5-FOA). Codirectional and Complementary chimaeric constructs in Figure 2B were ligated to the kanamycin resistance gene marker and transformed into the *S. pombe ura4-d18* strain. Transformants were selected on rich medium plates containing 100 μg/ml of G418 antibiotic. Chimaeric constructs in Figure 3 were ligated to the kanamycin resistance marker and used to replace the *SPACC11D3.16c* gene. The strain where the *ura4* gene replaced the endogenous *his7* gene was used to replace *ura4* by the modified *his7* gene after incorporating the +1N signature in the forward and reverse orientations by Crispr/Cas9 (Figure 4)[74]. Transformants were selected on plates with 5-FOA as above. Correct integration into the targeted *loci* in all the strains was confirmed by PCR and DNA sequencing. All the sequences of the constructs used in this work are shown in Figure S11).

Preparation of mononucleosomal and subnucleosomal DNA fragments and naked DNA controls

Mononucleosomal DNA was prepared from 200 ml of *S. pombe* cultures growing exponentially at 0.8 x 10^7 cells/ml. Cells were fixed with 0.5% formaldehyde for 20 min at room temperature. Glycine was added at 125 mM to stop the reaction and the cells were washed with water, resuspended in preincubation solution and treated with 8 mg of Zymolyase 20T for 20 minutes at 30 ºC to generate spheroplasts. Nucleosomes were released by digesting nuclei with a range of micrococcal nuclease (MNase) concentrations between 75 and 250 units/ml at 37 ºC for 45 minutes. The amount of MNase was optimized experimentally for each strain to generate an 80:20 ratio of mononucleosomes to dinucleosomes[50]. Samples were incubated at 65 ºC overnight to reverse the cross-linking in the presence of 1 mg/ml Protease K. Nucleosomal ladders were fractionated in 1.5% agarose and the 150 bp band of mononucleosomal DNA was recovered from the gel to construct the sequencing libraries. Libraries of mononucleosomal DNA were constructed following the Illumina protocol and were sequenced in an Illumina NextSeq500 platform using the paired-end protocol. We generated between 18 and 58 million reads per experiment, representing 186- to 582-fold genome coverage.

Naked DNA controls were prepared by extracting genomic DNA from the *S. pombe* strains in Figures 5 and 6 with the Blood & Cell Culture DNA Midi Kit (Qiagen). Naked DNA was digested with 1.2 units/ml of micrococcal nuclease (MNase) per microgram of DNA at 37 ºC for 10 minutes. Partially digested DNA was fractionated in a 1.5% agarose gel and the fraction corresponding to fragments 150 bp long (equivalent to mononucleosomal DNA) was recovered and processed to construct the sequencing libraries. Libraries of subnucleosomal DNA fragments were prepared as described by Henikoff et al.[49]

Alignment of sequence reads and DANPOS analysis

Reads were aligned using Bowtie[67] to the *S. pombe* genome (ASM294v2.20 assembly 13/08/2013 from PomBase [www.pombase.org]) or to genome versions where wild-type endogenous sequences were replaced by their modified counterparts (Figure S11). Alignment files were processed using the NucWave algorithm to generate the nucleosome occupancy maps and the frequency distribution of MNase cutting sites[69]. We estimated the difference in fuzziness between specific genomic regions using the *dpos* utility of the DANPOS 2 application[42] with a span of 1 bp and a read extension of 50 bp to make it compatible with NUCwave maps. We used the *profile* utility with a span of 1 bp to analyse the distributions of PRO-Seq counts of RNA polymerase II occupancy in the seven groups of nucleosomes in Figure 1B.

Chromatin immunoprecipitation and qPCR

Chromatin immunoprecipitation was performed as described by Pidoux et al.[75] with some modifications. Exponential *S. pombe* cells were fixed with 1% formaldehyde for 20 min at room temperature. Cells were disrupted in Fast Prep (Fp120, Savant Bio 101) (3 pulses of 1 minute at speed 4.5) and chilled on ice for 2–3 minutes between each disruption step. Cell extracts were sonicated in a Diagenode Bioruptor Sonicator Plus (4 cycles of 10 min each with alternating pulses of 30 sec on/off) to shear chromatin to a size range of

200–500 nucleotides. Samples were incubated overnight at 4 ºC with 1 μg of a monoclonal antibody against the CTD repeat (YSPTSPS) of the largest subunit of RNA polymerase II (ab26721-Abcam) for total RNAPII immunoprecipitation, or with 1 μg of polyclonal antibody against the phospho-Ser2 CTD repeat for elongating RNAPII immunoprecipitation (ab5095-Abcam). Samples were purified with the GFX PCR DNA and Gel Band kit (Cytiva). Immunoprecipitated chromatin and whole cell extract control samples were resuspended in 70 μl of sterile water before being used as a template for qPCR analysis. Primers were designed to amplify fragments of 70–90 nucleotides corresponding to the 5' and 3' regions of each transcript analysed as indicated in Figures 3A and 4A. To ensure PCR specificity in the chimaeric constructs in Figure 3, forward and reverse primers were designed to anneal to different nucleosomes adjacent in the construct but not in the genome.

RNA isolation, RT-qPCR and transcript stability

Total RNA was extracted with the RNeasy Kit (Qiagen). Strand-specific cDNA was synthesized using the Biotools High Retrotranscriptase-Starter Kit (Biotools) amplifying in each reaction the target cDNA and the normalizer cDNA (*S. pombe act1* gene) following the manufacturer's instructions. Each qPCR reaction was performed in at least three biological replicates.

To measure transcript stability, 30 ml of exponential cultures (DO645 = 0.8) of the different *S. pombe* strains were treated with 15 μg/ml thiolutin (Abcam) to inhibit RNA polymerase II.[66] Samples were taken at 0, 30, 60, 90, 120 and 180 minutes, pelleted and frozen in dry ice. RNA isolation and RT-qPCR analysis were performed as described above. Results at each time sample were normalized to the 0 time point and to 28S rRNA (*SPRRNA.47*) as an internal reference for transcript stability. RNA stability of *ura4* constructs was measured by removing glucose from the culture medium as described by Kim et al.[48]

RNA labeling and newly transcribed RNA purification

Labeling of nascent RNA with 4-thiouracil was performed as described[45]. Briefly, 100 ml of *S. pombe* cells were grown in YES medium at 32ºC to an $OD_{595} \approx 0.8$. Newly synthesized RNAs were labeled for 6 min by adding freshly prepared 4-thiouracil (Sigma-Aldrich) at a final concentration of 5 mM. In parallel, wild-type *S. cerevisiae* cells were grown in YPD medium, at 30º C and labeled for 6 min to be used as a spike-in control reference in all samples. After labeling, cells were immediately pelleted and *S. pombe* and *S. cerevisiae* cells were mixed at a ratio of 3:1. Mixed cells were frozen in liquid nitrogen and stored at -80º C. For non-labeling controls, *S. pombe* and *S. cerevisiae* cells were grown as described before, but only newly synthesized RNAs from *S. cerevisiae* cells were labeled. All the following steps were performed identically for the labeled and non-labeled *S. pombe* samples. Total RNAs were extracted using NZY Total RNA Isolation kit (NZYTech) according to the instructions of the manufacturer. RNA biotinylation was carried out using EZ-link HPDP- Biotin (Thermo Scientific™). Newly synthesized biotinylated RNAs were bound to 100 μL of μMACS streptavidin microbeads (Miltenyi Biotec) for 90 min at room temperature with gentle shaking. Purification of labeled RNA was then carried out using μMACS streptavidin starting kit (Miltenyi Biotec) as described in[45].

QUANTIFICATION AND STATISTICAL ANALYSIS

Identification of nucleosome groups along transcription units

We used the *S. pombe* and *S. cerevisiae* maps of nucleosome occupancy reported by González et al.[36] to extract the position of the nucleosome dyads. Maps for *Schizosaccharomyces octosporus* and *Schizosaccharomyces japonicus* were described by Quintales et al.[35] and those for *Candida albicans* were generated for this work following the same protocol as for *S. pombe*. The identification of well-positioned nucleosomes was performed as described by Quintales et al.[35] They were defined as peak positions whose level of occupancy was 1.4-fold above the average genome occupancy and the nearest maximum on each direction was at least 150 nucleotides away. According to this criterion, we selected 49,998 well-positioned nucleosomes in *S. pombe*, 32,246 in *S. cerevisiae*, 41,678 in *S. octosporus,* 21,006 in *S. japonicus* and 29,744 in *C. albicans*. We identified +1 (+1N) and terminal (TN) nucleosomes by selecting those overlapping with TSS and TTS. *Schizosaccharomyces pombe* TSS were obtained from the Deep-CAGE analysis by Li et al.[76]. The analysis was expanded to genes not present in that study by RNA-seq data from our lab. Altogether, we identified 4474 +1 nucleosomes in *S. pombe*, amounting to 88% of all the annotated coding genes in the genome. For TN, we selected nucleosomes overlapping the 2839 TTS positions identified by Lantermann et al.[50] For *S. cerevisiae* we used the TSS (3613 genes) and TTS (3157 genes) described by Nagalakshmi et al.[77]. TSS for *S. octosporus* and *S. japonicus* were reported by Rhind et al.[78] and those for *C. albicans* were taken from the Candida Genome Database. Central nucleosomes (CN) were identified as those overlapping the central position between TSS and TTS (3248 for *S. pombe* and 3826 for *S. cerevisiae*). +2N and +3N nucleosomes were selected by their adjacent position downstream from +1N (3442 and 2731 for *S. pombe* and 3561 and 2339 for *S. cerevisiae*) and TN-2 and TN-3 nucleosomes as those immediately adjacent upstream from TN (1179 and 661 for *S.pombe* and 1768 and 788 for *S.cerevisiae*). All selected nucleosome groups were mutually exclusive.

Generation of nucleotide profiles along nucleosomal DNA

Nucleosomal DNA sequences 150 bp long associated with well-positioned nucleosomes of the seven groups in Figure 1A and Figure S1 were aligned to the dyad position following the directionality of transcription (except for genome average panels in Figure 1A).

Base composition profiles were generated by computing the frequency of each nucleotide at each position. For representation purposes, the frequency shown at each position is the mean frequency for a 20 nt window (or smaller in the case in the latest 20 positions) starting at such position.

Statistical analysis

t-Student p values were calculated using the GraphPad QuickCalcs (https://www.graphpad.com/quickcalcs/ttest1/). p-values of all the qPCR and ChIP analysis in Figures 3 and 4, S5 and S9 are shown in Table S2. Standard deviation was calculated using Excel. Kolmogorov-Smirnov (K-S) test p values in Figures 5, 6, and S10 were calculated using R.

Incorporation of nucleosomal signatures in the *his7* and *ura4* ORFs sequences by codon substitution

Nucleosomal signatures[35,36] are defined as a 150 x 16 numerical position-specific weight matrix (PSWM) F where F_{ij} is the frequency of dinucleotide j at position i, log2 normalized by the whole genome frequency of dinucleotide j:

$$F_{ij} = log_2\left(\frac{freq(j,i)}{genfreq(j)}\right)$$

To generate the PSWM of *S. pombe* +1 nucleosomes we aligned the sequences of 4474 +1 nucleosomes to their dyad position in the direction of transcription. We extracted the genomic sequences from PomBase (www.pombase.org) (ASM294v2.20, assembly 13 August 2013). This directional signature was incorporated into each nucleosome of the *ura4* and *his7* ORFs separately, conserving the wild type sequence of the three nucleotides of the linkers intact. The incorporation was done by maximizing the dinucleotide frequencies based on the PSWM allowed by the synonymous codons to maintain amino acid composition of the wild type ura4 and his7 proteins. Let *ABC* be a codon located at position *i* within nucleosomal DNA, where *AB* and *BC* are the two overlapping dinucleotides of the codon. Let {*ABC*} be the set of all *ABC* synonymous codons. The new codon *XYZ* incorporating the signature will be *rem*(*ABC*,*i*):

$$rem(ABC,i) = XYZ; max(F_{XYi} + F_{YZi+1}) \forall XYZ \in \{ABC\}$$

For the *ura4* and *his7* ORF sequences, we selected the nucleosome positions described by González et al.[28] Nucleosomes 1 and 6 of *ura4* and 1 and 9 of *his7*, encompass the boundaries of their ORF sequences (Figure 4A) and only the sequences within the ORF were modified according to their position along the 150 nucleotides of the PSWM. The incorporation of signatures into ORFs was programmed into a python3 script called *remaster.py* that computes nucleosomal signatures and incorporates them into ORF sequences. The script is freely available at GitHub under a GPL 3.0 License (https://github.com/rodrigoSantamaria/remaster). The commands used to generate the modified ura4 and his7 sequences in Figure 4 are described in the website above.